Phytoplanktonic Response to simulated Volcanic and Desert Dust Deposition Events in the South Indian and Southern Oceans

Carla Geisen[1], Céline Ridame[1], Emilie Journet[2], Pierre Delmelle[3], Dominique Marie[4], Claire Lo Monaco[1], Nicolas Metzl[1], Rawaa Ammar[2,3], Joelle Kombo[1], Damien Cardinal[1]

[1]Sorbonne Université, LOCEAN – IPSL Laboratoire d'Océanographie et du Climat: Expérimentations et Approches Numériques, UMR 7159, (SU CNRS MNHN IRD), 75252 Paris Cedex 05, France. [2]LISA (Laboratoire Interuniversitaire des Systèmes Atmosphériques), UMR 7583, CNRS, Université Paris-Est Créteil et Université de Paris, Institut Pierre Simon Laplace (IPSL), Créteil, France. [3]Earth and Life Institute, Environmental Sciences, UCLouvain, B-1348 Louvain-la-Neuve, Belgium. [4]CNRS, Sorbonne Université, UMR 7144 Adaptation et Diversité en Milieu Marin, Station Biologique de Roscoff, 29680 Roscoff, France.

Corresponding author: Carla Geisen (carla.geisen@locean.ipsl.fr)

Key Points:

- Representative desert dust and volcanic ash depositions released significant amounts of Fe and Si but not NOx to seawater.
- The triggered phytoplankton response was mainly caused by diatom development.
- The Kerguelen plateau presented the highest response in primary production, despite being naturally fertilized.

Abstract

We conducted microcosm incubation experiments in contrasting biogeochemical areas of the South Indian Ocean and Indian sector of the Southern Ocean to determine the phytoplankton response to aerosol related nutrient release. Dry depositions of 2 $mg.L^{-1}$ of dust from Patagonia or 25 $mg.L^{-1}$ of ash from the Icelandic stratovolcano Eyjafjallajökull were added to trace metal clean incubations of surface seawater, along with nutrients (Si, Fe, N or P) at five stations. We interpreted the biological response based on abiotic experiments of aerosols nutrient release. We showed that both types of aerosols increased significantly the primary production by resolving some main local nutrient limitations of the Southern Ocean, at least for iron and to a lesser extend for silicon. Phytoplanktonic communities reacted differently to the additions; however added nutrients/aerosols were mostly beneficial for diatom growth, responsible for 40 to 100 % of the algal biomass increase, depending on the region and aerosols. Nonetheless, the aerosols did not relieve main N limitation of the LNLC area, as neither dust nor ash released significant amounts of NOx. According to these findings, characteristic localized high deposition of volcanic eruptions be of equal or higher importance to phytoplankton compared to desert dust, despite ashes' lower nutrient solubility to the ocean.

Plain Language Summary

The South Indian and Southern Oceans are known for contrasting nutrient concentrations and different microalgal communities, limited by the low content of several nutrients. In most of this area, nutrients are supplied by oceanic interfaces (aerosols, sediments, ice…). Only limited amounts of atmospheric dust reach currently the remote open ocean, but aerosol deposition nevertheless constitutes one of the major sources of new nutrients within this vast ocean area. This supply might have dramatically changed with time compared to glacial times and/or volcanic eruption events. After deposition on the sea surface, the particles release nutrients such as iron and silicon to the seawater, which might temporally boost algal development.

In this study, we show that a representative deposition of desert dust or volcanic ash triggers a biological response in different regions of the Indian Southern Ocean. Some algae groups such as diatoms benefit more from the new nutrients, thereby modifying the structure of the planktonic community. On the other hand, the same deposition had no effect in the central part of the South Indian Ocean, as the local nitrogen limitation was not relieved by the aerosols.

1 Introduction

The Southern Ocean (SO) is the most extended High Nutrient Low Chlorophyll (HNLC) area of the world ocean, where phytoplankton growth is mostly limited by low iron (Fe) surface concentrations (Martin, 1990; Moore et al., 2002). Moreover, due to latitudinal gradients of dissolved macronutrients decreasing northwards, the SO can be subdivided in several biogeochemical regions with different nutrient limitations. In the Subantarctic Zone (SAZ), which is North of the subantarctic front (SAF) and south of the subtropical front (STF), dissolved silicon (dSi) becomes scarce (Nelson et al., 2001), shifting the Fe limitation of the Antarctic Zone (AZ) towards a Fe/Si co-limitation (Hoffmann et al., 2008; Hutchins et al., 2001). Further north, the STF signs the boundary towards the Low Nutrient Low Chlorophyll (LNLC) area of the Subtropical Zone (STZ) of the South Indian Ocean (SIO) with low dissolved inorganic phosphorus (DIP) and NOx (NO_3^- + NO_2^-) within the oligotrophic subtropical gyre (McClain et al., 2004; Morel et al., 2010).

One of the factors responsible for the SO Fe-depletion is the scarcity of so-called new Fe supply, *i.e.* Fe reaching the euphotic zone from reservoirs outside this surface layer. The fluvial input can be neglected in the remote SO (Middag et al., 2011), making atmospheric aerosol deposition the main Fe source (Cassar et al., 2007; Chester and Jickells, 2012), except in upwelling areas associated with hydrothermal vents (Ardyna et al., 2019), in areas subjected to Fe-rich sea ice melting (Vancoppenolle et al., 2013) or within the naturally fertilized coastal regions such as the Kerguelen and Crozet plateaus (Blain et al., 2007; Planquette et al., 2007), as emphasized by Tagliabue et al. (2017) for high-latitudes. While current monthly averaged dust deposition to the SO is very low (Meskhidze et al., 2007), daily peaks of intense episodic events well above the lower monthly averages could sporadically affect phytoplankton, especially during the austral summer months, when the water column is stratified and the number of dust days detected from the Patagonian source area is maximal (Gassó and Torres, 2019). While the present-day dust supply to the modern SIO and SO is extremely low (Grand et al., 2015b; Jickells et al., 2005; Piketh et al., 2000; Tagliabue et al., 2008), several studies suggested that dust deposition to the SO was up to 20 times higher during the last glacial maximum (Conway et al., 2015; Mahowald et al., 1999). These periods of increased Fe supply by dust might partly explain millennial-scale CO_2 fluctuations and glacial-interglacial cycling. Indeed, during glacial intervals, the higher dust Fe supply could have triggered higher phytoplanktonic productivity and a more efficient

biological carbon pump in the SO and ultimately a global atmospheric CO_2 drawdown (Conway et al., 2015; Martin, 1990; Watson et al., 2000). Thus, the role of atmospheric particles as source of new nutrients to the surface SO is important in the climate feedback, along with their ability to scatter solar radiation (Tegen and Schepanski, 2018).

Significant CO_2 drawdowns have also been observed on local and regional scales after past and modern volcanic eruptions (Langmann et al., 2010a), suggesting possible equivalent fertilization of remote open ocean areas by volcanic ash compared to desert dust (Duggen et al., 2010; Langmann et al., 2010b). However, the range of ash deposition is highly variable (Durant et al., 2010) and may be influenced by a wide variety of parameters such as the magnitude of the eruption, the ash emission rate of the volcano, the wind speed and direction, particle aggregation processes within the ash cloud, as well as the distance between source and deposition site (Duggen et al., 2010).

Over the last decades, several mesoscale artificial Fe enrichment experiments (Boyd et al., 2007 and references therein) have demonstrated the relieve of phytoplankton growth limitation after the addition of Fe to the SO, while microcosm studies were able to show a biological response after dust or ash additions to the Atlantic sector of the SO (Browning et al., 2014; Trimborn et al., 2017). Yet the SIO and Indian SO represents an important ocean basin where biogeochemical experiments remain scarce. One of the novelties of our study is the direct comparison of volcanic ash and desert dust nutrient release and bioavailability in different HNLC and LNLC areas of the SO. In addition, we compare the biological response to both dry and wet deposition modes, well-known to influence nutrient solubility (Chester and Jickells, 2012; Duggen et al., 2010).

2 Materials and Methods

2.1 Cruise transect, hydrological and biogeochemical context

Since 1998, physico-chemical and biogeochemical parameters were measured at least once a year in the SIO and SO (20° S–60° S) in the frame of the French OISO (Ocean Indien Service d'Observations) program. The following study was conducted as part of the VT163/OISO-29 (MD217) cruise (Metzl and Lo Monaco, 2020), on board the R/V *Marion Dufresne*, which took place in the SIO and SO during the austral summer, from the 5th of January to the 15th of February 2019 (Fig. 1). Nutrient/aerosol additions during bioassay experiments were performed

110 at five stations (2, 11, A3, 14 and 16, Fig. 1), located in contrasted biogeochemical regions. The
111 oceanic area studied in the frame of the OISO program is characterized by latitudinal gradients
112 of sea surface temperature and salinity (SST and SSS, respectively) decreasing southward and of
113 macronutrients increasing southward (Jabaud-Jan et al., 2004; Metzl et al., 2006). Stations 2 and
114 16 are located in the southwest Indian subtropical gyre in the STZ north of the STF. The STZ is a
115 LNLC region, characterized by warm and oligotrophic surface waters. Station 14 lies south of
116 the STF and north of the SAF within the SAZ, a transition zone between the macronutrient-poor
117 STZ and the macronutrient-rich AZ. The SAZ is characterized by high nitrogen (N) and
118 phosphorous (P) but low silicon (Si) and Fe concentrations (Hutchins et al., 2001), and described
119 by Dugdale and Wilkerson (1998) as a High Nitrate-Low Silicate-Low Chlorophyll (HN-LSi-
120 LC) region. Station 11 is situated south of the polar front (PF), within the vast High Nutrient (N,
121 P, Si) Low Chlorophyll (HNLC) area of the AZ separated from the SAZ by a strong SST
122 gradient across the PF (Moore et al., 1999). Lying also below the PF, A3 is a reference station of
123 the diatom bloom area at the naturally Fe-fertilized Kerguelen plateau (Blain et al., 2007; Fripiat
124 et al., 2011b).

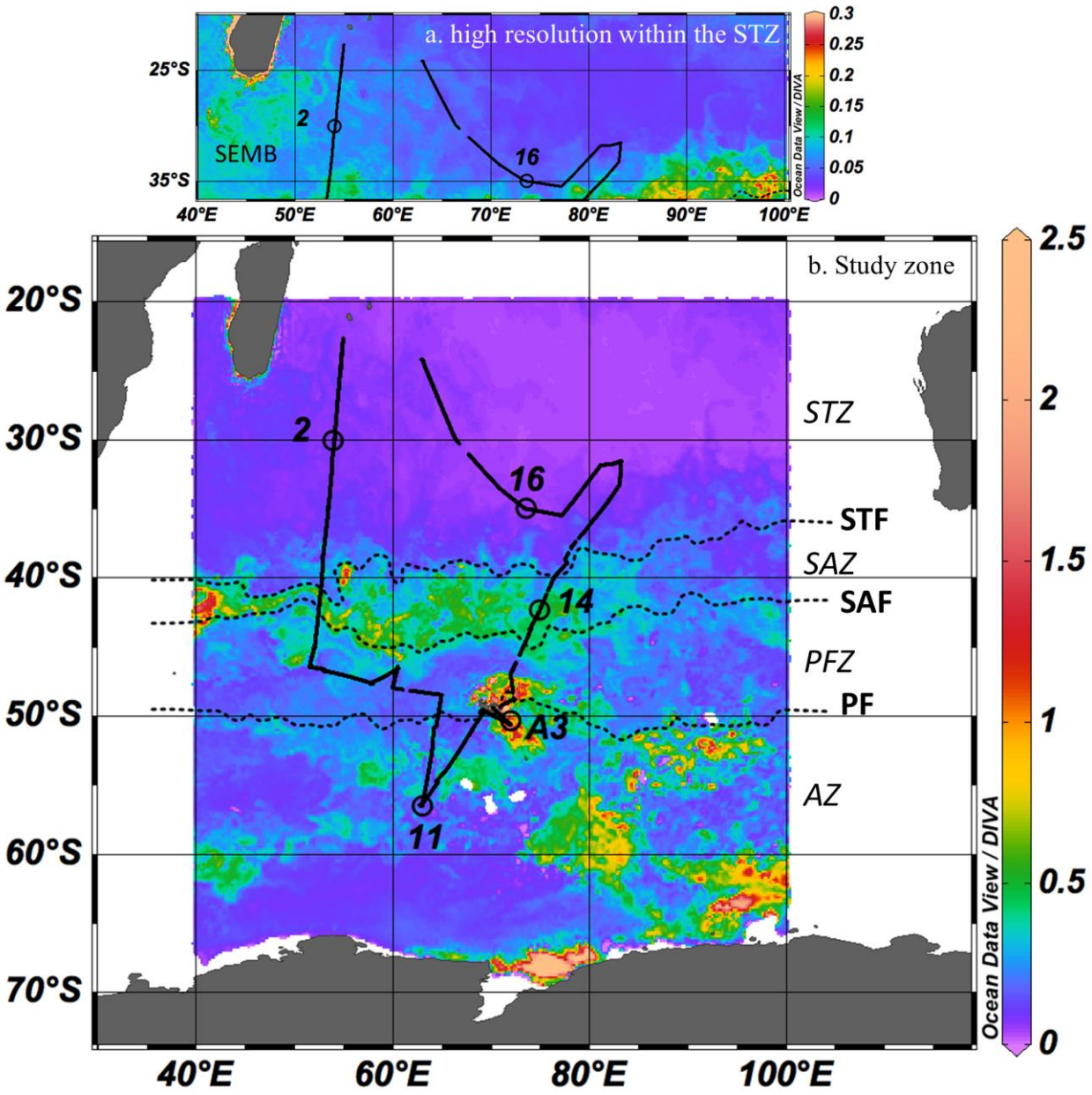

Figure 1. OISO-29 cruise transect with the locations of the five stations (2, 11, A3, 14 and 16) where bioassay experiments were performed, and satellite-derived chlorophyll-a concentration (µg.L-1) averaged over January 2019 (MODIS). The position of major fronts was determined from satellite-derived temperature data (January 2019, MODIS): STF: subtropical front (18 °C), SAF: subantarctic front (13 °C) and PF: polar front (5 °C). Fronts delimit the STZ: subtropical zone, SAZ: subantarctic zone, PFZ: polar front zone and AZ: Antarctic zone. The map (a) shows the STZ with a higher resolution than the general map (b), thus enabling the detection of the South East Madagascar bloom (SEMB). Figures were produced using Ocean Data View (Schlitzer, 2021).

2.2 Bioassay experiments

All materials were acid-washed (HCL Suprapur) and manipulations took place under laminar flow hoods. Unfiltered surface seawater (~10 m depth) was collected within the surface mixed layer using Go-Flo bottles and Kevlar wire to avoid any metallic contamination. We carried out trace metal clean nutrient and aerosol additions during bioassay experiments at five stations (Fig. 1), characterized by contrasted biogeochemical features. Bioassays were performed in two sets of acid cleaned polycarbonate bottles per replicate, with 4.5 L bottles dedicated for biogenic silica measurement and 2.3 L bottles for all other biological samples.

Table 1. Experimental nutrient and aerosol additions at each station. At station 11, simulated dry and wet deposition events were performed.

Station	Zone	Region	+Dust	+Ash	+Fe	+Si	+FeSi	+N	+NP
2	**STZ**	LNLC	dry	dry	x	x	x	x	x
16	**STZ**	LNLC	dry	dry	x	x	x	x	x
14	**SAZ**	HN-LSi-LC	dry	dry	x	x	x		
A3	**AZ**	Kerguelen plateau	dry	dry	x	x	x		
11	**AZ**	HNLC	dry/wet	dry/wet	x				

Experimental nutrient additions were adapted to potential nutrient limitations of each type of biogeochemical region (Table 1). We performed mono- and multiple nutrient additions: +Fe: 2 $nmol.L^{-1}$ $FeCl_3$; +Si: 2 $\mu mol.L^{-1}$ Na_2SiO_3; +FeSi: 2 $nmol.L^{-1}$ $FeCl_3$ + 2 $\mu mol.L^{-1}$ Na_2SiO_3; +N: 2 $\mu mol.L^{-1}$ $NaNO_3$; +NP: 2 $nmol.L^{-1}$ $NaNO_3$ + 0.2 $\mu mol.L^{-1}$ KH_2PO_4. Possible trace metal contamination from the added nutrient solutions has been measured by ICP-AES and is discussed in the supplementary material S1. One unamended sample was used as a control. In addition to nutrient enrichments, dry deposition events of desert dust and volcanic ash were simulated by adding aerosols at final particle concentrations (PC) of 2 $mg.L^{-1}$ for the dust treatment (+dust) and of 25 $mg.L^{-1}$ for the ash treatment (+ash) (see Table 2 for composition of aerosols and section 2.4.2 for justification of PC). Each nutrient/aerosol treatment was performed in triplicate.

157 At the HNLC station 11, wet deposition events of ash and dust were also simulated. Artificial
158 rainwaters (ARW) were prepared following the protocol described in Paris et al. (2011). Briefly,
159 aerosols were added to ultrapure water (Millipore®, resistivity of 18.2 $M\Omega.cm^{-1}$) previously
160 acidified with sulfuric acid (1‰ H_2SO_4 SupraPur® at 2.10^{-2} M, theoretical pH of 4.7), which is
161 naturally found in the atmosphere (Pye et al., 2020). After a contact time of 60 min in ARW (PC
162 of 100 $mg.L^{-1}$ dust and 1250 $mg.L^{-1}$ ash), 2 % of unfiltered ARW was added to the incubation
163 bottles filled with unfiltered surface seawater, in order to obtain the same PC as in the dry
164 deposition experiments (2 and 25 $mg.L^{-1}$ for respectively dust and ash). In order to determine the
165 chemical composition of ARW, aliquots were filtered through a 0.2 µm polycarbonate
166 membrane for measurements of the macronutrients and dissolved iron concentrations (see
167 section 2.5 for analysis).
168 After nutrient/aerosol additions, the microcosms were placed in on-deck incubators for 48 h with
169 circulating surface seawater and covered by a filter to simulate the appropriate irradiance
170 encountered at 10 m depth. Before the nutrient/aerosol additions, seawater was sampled for
171 initial determination of the primary production, pigments, cell abundances, biogenic silica (bSi),
172 macronutrients and dissolved Fe (dFe) concentrations. Samples for pigments, bSi, cell abundance
173 and nutrients were collected at final time (48 h) in all the treatments, and the primary production
174 was determined between 24 h and 48 h.

175 ## 2.3 Abiotic dissolution

176 Nutrients released by dust and ash were monitored at each station with an abiotic control of 0.2
177 µm filtered surface seawater (SW), using the same deposition mode (dry event at all stations and
178 wet event at HNLC station 11) and aerosol PC as in the bioassay experiments. Triplicates of 250
179 mL polycarbonate bottles were placed in the same experimental conditions than microcosms and
180 harvested after 48 h for macronutrients and dFe concentrations. For back-calculations of Fe
181 release in ash ARW (see section 2.5), we used supplementary samples filtered after 12 h.

182 ## 2.4 Characterization of dust and ash

183 ### 2.4.1 Collection and composition

184 Collection took place in remote areas using clean sampling techniques. Samples were stored in
185 double zip bags to avoid anthropogenic contamination.

Desert dust

The fine fraction (< 20 µm) of a Patagonian arid surface soil (south of Sierra Grande, Argentina, hereafter referred to as Pata) was used for the dust additions at the five stations. The soil sample was collected from the first centimeters of the top layer of the desert soils, exposed to wind erosion and dry sieved in order to produce a dust analogue (Guieu et al., 2010), hereafter referred to as aerosol for simplification, according to a protocol described by Guieu et al. (2014). Dust from this region has been shown to reach the Southern Ocean (Gili et al., 2016; Li et al., 2008; Mahowald, 2007; Smith et al., 2003).

Volcanic ash

The ash originated from the 2010 explosive eruption of Eyjafjallajökull volcano (63°37'11" N, 19°36'54" W) in Iceland, hereafter referred to as Eyja. The ash was collected on the ground immediately after an ash fall event that occurred in Holtsa (~4–5 km from the volcano) on 17 April. The ash sample was sieved at 100 µm to remove large particles that are not representative of the material transported over long distances in the atmosphere (Gudmundsson et al., 2012; Rose and Durant, 2009; Witham et al., 2005). Thus, the Eyja ash is not directly representative of volcanic ash deposition over the modern SIO and the SO, but was the best available sample for our study.

The chemical and mineralogical composition of Pata and Eyja are presented in Table 2. Carbon (C) and N were quantified with an isotope ratio mass spectrometer (IR-MS Delta V plus, Thermo Fischer Scientific) coupled with a C/N analyzer (Flash EA, Thermo Fisher Scientific). P, Si and Fe were measured after acid digestion (Fu, 2018) with inductively coupled plasma mass spectrometry (ICP-MS 7500cx, Agilent) or with ICP after fusion (Thermo Fischer Scientific). The median diameter was calculated from volume size distribution measured by laser diffraction in ultrapure water (without ultra-sonication to avoid breaking up aggregates). Specific surface area (SSA) was determined by the Brunauer, Emmet and Teller (BET) gas adsorption method using nitrogen for dust (< 20 µm) and krypton for ash particles (< 100 µm). The mineralogical composition of the crystalline portion of aerosols was measured by quantitative X-ray diffraction (XRD) and the proportion of the amorphous phase was determined by adding an internal standard.

2.4.2 Representativeness of aerosol depositions

Desert dust

Studies based on satellite data (Erickson et al., 2003; Gassó and Torres, 2019), modelling (Li et al., 2008; Mahowald, 2007) and ice core analyses (McConnell et al., 2007) have revieled Patagonian dust deposition in Antarctica and the SO. The chosen PC from this study (2 $mg.L^{-1}$), corresponds to an estimated deposition of 9 $g.m^{-2}$ (see Supplementary Material S2). Local dust deposition rates are extremely low (potential maxima at 45° S in the Atlantic sector of the SO with an annual mean deposition of 8.0 $mg.m^{-2}.day^{-1}$ calculated according to Li et al. (2008). Thus, this deposition rate is not realistic for modern atmospheric deposition in the SOI and SO, but remains representative for other time periods and other offshore oceanic areas: the SO received up to 20 times higher dust deposition during the Last Glacial Maximum (Conway et al., 2015; Mahowald et al., 1999), and high Saharan dust deposition events reach up to 22 $g.m^{-2}$ in the modern open Mediterranean Sea (Ternon et al., 2010). The chosen PC is also in agreement with several bioassay studies performed in the Mediterranean Sea, Atlantic and Pacific Ocean, in which dust PC of 2 $mg.L^{-1}$ has been used (*e.g.* Jacq, 2014; Marañón et al., 2010; Mélançon et al., 2016; Mills et al., 2004).

Volcanic ash

The global deposition flux of volcanic ash is less studied than desert dust flux and there is to date no available annual estimate of deposition to the SO and SIO. Ash fluxes to the ocean are strongly less frequent than desert dust events (Durant et al., 2010) and usually unpredictable eruptions might lead to the deposition of great ash masses over the ocean (Langmann, 2013). In this study, we used an ash PC of 25 $mg.L^{-1}$, corresponding to an estimated deposition of 300 $g.m^{-2}$ *i.e.* a realistic 0.2 mm ash layer (see Supplementary Material S2). Thus, the ash PC is at the same order of magnitude than the published estimates of historical eruptions, as well as other bottle experiments (6.0 to 35.8 $mg.L^{-1}$ of ash in the Atlantic sector of the SO in Browning et al. 2014).

2.5 Biological and chemical parameters

Primary Production

Net CO_2 fixation rates were determined using the ^{13}C-tracer addition method. 1 mL of $NaH^{13}CO_3$ (99 %, Eurisotop) was added 24 h after the beginning of incubation to fully filled 2.3 L experimental polycarbonate bottles. Then, the bottles were vigorously shaken after spike addition, and placed back into on-deck incubators for 24 h. After incubation, 1 L to 2.3 L were gently filtered onto pre-combusted 25 mm Whatman GF/F filters and stored at -80 °C. Sample filters were dried at 40 °C for 48 h before analysis. Carbon in particulate matter and ^{13}C isotopic ratios were quantified using an online continuous flow elemental analyzer (Flash 2000 HT), coupled with an Isotopic Ratio Mass Spectrometer (Delta V Advantage via a conflow IV interface from Thermo Fischer Scientific).

Cell abundance

The cell abundances of heterotrophic bacteria, cyanobacteria pico- and nanoeukaryote species (< 30 µm) were determined by flow cytometry according to the protocol detailed in Marie et al. (1999). Briefly, 1.5 mL of seawater were immediately fixed with 15 µL of glutaraldehyde (25 %) and placed in the dark for 15 min before being frozen and stored at -80 °C.

Pigments

One to two liter of seawater were filtered onto GF/F filters at initial time and after 48 h incubation, then immediately placed at -80 ºC prior to analysis at the SAPIGH analytical platform at the Institut de la Mer (IMEV, Villefranche-sur-Mer, France). Filters were extracted at -20 ºC in 2 mL methanol (100 %) containing an internal standard (vitamin E acetate, Sigma©), disrupted by sonication and clarified one hour later by vacuum filtration through GF/F filters. The extracts were rapidly analyzed (within 24 h) on a complete Agilent© Technologies 1200 series HPLC system. The general procedure for HPLC pigment analysis, identification and quantification were described in Ras et al. (2008). HPLC sampling at final time at LNLC stations (2 and 16) could not be carried out because the volume of seawater available after the sampling of other parameters (PP, nutrients, etc.) was insufficient. Taxonomic pigments were used as size class markers of phototroph groups (pico-, nano- and microphytoplankton). The chemotaxonomic correspondence of HPLC-determined pigments and the associated size-class

came from Uitz et al. (2006). The biomass fractions of the three phytoplankton size classes was calculated with the following equations from Uitz et al. (2006):

$$f_{micro} = (1.41\ Fuco + 1.41\ Peri)/wDP \quad (1a)$$

$$f_{nano} = (1.27\ 19'HF + 0.60\ Allo + 0.35\ 19'BF)/wDP \quad (1b)$$

$$f_{pico} = (0.86\ Zea + 1.01\ Tchlb)/wDP \quad (1c)$$

where *wDP* is the weighted sum of the concentrations of the seven diagnostic pigments:

$$wDP = 1.41\ Fuco + 1.41\ Peri + 1.27\ 19'HF + 0.60\ Allo + 0.35\ 19'BF + 0.86\ Zea + 1.01\ Tchlb \quad (2)$$

The concentration of total chlorophyll-a (Tchla) associated with each size class was calculated as follows, with *x* standing either for *micro*, *nano* or *pico*:

$$Tchla_x = f_x \times Tchla \quad (3)$$

The diatom and dinoflagellate biomass were estimated as follows:

$$Chla_{diatom} = (1.41\ Fuco * Tchla)/wDP \quad (4a)$$

$$Chla_{dinoflagellate} = (1.41\ Peri * Tchla)/wDP \quad (4b)$$

The relative contribution of each size class to the increase in Tchla ($\Delta Tchla_x$, in %) in the nutrient/aerosol treatment *(trtm)* after 48 h relative to the mean control *(ctr)* after 48 h was calculated as follows:

$$\Delta Tchla_x = \frac{Tchla_x(trtm.48h) - Tchla_x(mean\ ctr.48h)}{Tchla(trtm.48h) - Tchla(mean\ ctr.48h)} \times 100 \quad (5)$$

Biogenic silica

Samples for bSi were collected at initial time and after 48 h incubation through gentle filtration of 1 or 1.5 L (depending on local potential diatom abundance) from the 4.5 L incubation bottles on 47 mm polycarbonate membrane Nucleopore (0.8 µm) filters using 1 L Nalgene filtration units (Thermo Scientific™). As described in Fripiat et al. (2011), the filters were stored in polycarbonate Petri dishes and dried on board at 60 °C overnight, then stored at room temperature until on shore analysis. The bSi was extracted from the membrane filter through alkaline digestion following a protocol adapted from the first leaching step found in Ragueneau et al. (2005). Briefly, the bSi was dissolved in 4 mL NaOH solution (0.2 M, pH 13.3) during 40 min at 100 °C, after which the solution was neutralized with 1 mL Suprapur HCl (1 M) or 0.8 mL Suprapur HNO_3 (1 M) to stop the digestion. The leachate was analyzed for Si concentration by spectrophotometry (Thermo Fisher Evolution 220) using the manual colorimetric method of

Grasshoff et al. (1999). As some lithogenic silica (LSi) might also dissolve during the digestion, the aluminum (Al) concentration of the leachate was measured by ICP-MS (Agilent 7900). We used the mean crustal Si/Al ratio of 3.74 (Taylor and McLennan, 1985) to correct the measured Si concentration from lithogenic contamination:

$$[bSi] = [Si] - [Al] \times 3.74 \quad (6)$$

Note that bSi samples after 48 h of incubation were analyzed in duplicates only, while we performed replicated measures of subsamples and/or analytical replicates for the initial sample from each station. Biogenic Si in dust and ash treatments are not shown, since the high LSi proportion from the aerosols overwhelms the bSi signal, yielding to a much too large uncertainty of the correction. Despite a higher filtration volume (1.5 L instead of 1 L), bSi at LNLC stations (2 and 16) was below detection limit (0.01 µmol.L^{-1}).

Macronutrients

Samples of dSi, DIP and NOx were obtained through 0.2 µm filtration as follows: (1) for initial conditions, SW samples were directly filtered on-line from the Go-Flo bottles through acid-cleaned 0.2 µm capsule filters (Sartorius Sartobran-P-capsule 0.45/0.2 µm); (2) at 48 h in the abiotic experiments, SW samples were filtered onto acid-cleaned PALL Supor 0.2 µm polyethersulfone (PES) filters mounted on polyethylene syringes; (3) the same 0.2 µm filtration protocol was performed after 1 h of contact with ARW. Samples were stored at +5 °C (dSi) or -20 °C (DIP and NOx) prior to on shore analysis. Dissolved Si and DIP were measured with a spectrophotometer (Thermo Fisher Evolution 220) according to the manual colorimetric methods of Grasshoff et al. (1999) and Murphy and Riley (1962), respectively. The concentration of NOx was measured with the SEAL AutoAnalyzer 3HR, according to Aminot and Kérouel (2007). The detection limits were 0.03 µM dSi, 0.03 µM DIP and 0.08 µM NOx.

Micronutrients

The same 0.2 µm-filtration protocol than for macronutrients was used for dissolved iron (dFe), manganese (dMn) and cobalt (dCo) samples in SW. After filtration (with acid cleaned capsule or syringe/filters), micronutrient samples were acidified (0.2 % HCl Ultrapur) and stored at +5 °C before analysis by ICP-MS coupled with an automated sample preconcentration system (SeaFAST) according to Wuttig et al. (2019). The detection limits in SW were 0.005 nM dFe,

329 0.016 nM Mn and 0.2 pM dCo. Moreover, dFe in ARW after 1 h was measured by ICP-AES
330 (Spectro Arcos) with a detection limit of 8.0 nM dFe. Due to Fe contamination issues of the ash
331 ARW samples during analysis, we estimated the Fe release and resulting solubility in ash ARW
332 according to a back-calculation of dFe release after the addition of 2 % ash-containing ARW to
333 the abiotic filtered SW control:

334 $$\mathrm{dFe_{ARW}} = \Delta \mathrm{dFe_{SW.12h}}/0.02 \quad (7)$$

335 where $dFe_{SW.12h}$ corresponds to the first available data point 12 h after addition of 2 % ARW in
336 0.2 µm-filtered SW. The calculated concentration might be biased by secondary Fe release
337 and/or scavenging processes during the 12 h in the SW matrix.

338 **Calculation of nutrient and aerosol induced responses**

339 In order to compare the biological response in the different bioassay treatments at the five
340 stations, we calculated the relative change (RC) of each parameter according to:

341 $$RC\ (in\ \%) = (C_{trmt.48h} - C_{ctr.48h}) \times 100/C_{ctr.48h} \quad (8)$$

342 where C_{trtm} stands for the concentration of the variable (primary production, cell abundance,
343 pigments, bSi) 48 h after the nutrient/aerosol addition and C_{ctr} is the mean value of the variable
344 in the control after 48 h.

345 **2.6 Statistical analysis**

346 Means (n=3) after 48 h incubation in the bioassay as well as in the abiotic experiments were
347 compared using a one-way ANOVA followed by a Fisher LSD means comparison test. When
348 assumptions for ANOVA were not respected, the tests were performed on the log-transformed
349 data or means were compared using a Kruskal–Wallis test and a post hoc Dunn test. Means of
350 nutrient solubility for dust and ash in the abiotic experiments were compared using the Student's
351 t-test. Statistical tests were done using the XLSTAT software.

3 Results

3.1 Characterization of aerosols and nutrient release

3.1.1 Composition of aerosols

The two tested aerosols have a different mineralogy and elementary composition (Table 2). The Pata dust is richer in C and N but lower in P and Fe relative to the Eyja ash. The Si content is similar for both aerosols. Dust particles (sieved < 20 µm) had a nine times higher specific surface area (SSA) than the larger (sieved < 100 µm) ash particles. Pata dust contains twice more clay, while Eyja ash is more amorphous *i.e* contains less crystalline minerals. Compared to Saharan dust, which usually contains less than 10 % of feldspars (Journet et al., 2008), the Pata dust is enriched in magmatic silicate minerals, including albite (18.6 wt.%, Table 2), originating from the eruptive products of nearby volcanos (Simonella et al., 2015).

Table 2: Mineralogical and chemical properties (% in weight) of the fine fraction of the Patagonian soil (< 20 µm) and the volcanic ash (< 100 µm) used in the bioassay and abiotic experiments.

		Desert Dust (Pata)	**Volcanic Ash (Eyja)**
Origin		Sierra Grande Patagonia	Eyjafjallajökull Iceland
Mineralogy (%)	Lime stones	calcite 2.9	calcite 0.3
	Acidic rocks	albite 18.6; quartz 6.2	albite 23.4; analcime 1.0
	Clays	illite 20.6; smectite 2.8	smectite 10.9
	(hydr)oxides	not detected	gibbsite 0.3; hematite 0.1
	amorphous	48.3	63.7
Specific surface area ($m^2.g^{-1}$)		62.1	7.3
	C (%)	1.06 ± 0.01	0.14 ± 0.01
	N (%)	0.09 ± 0.01	0.03
	P (%)	0.08 ± 0.01	0.18 ± 0.01
	Si (%)	25.8	26.47
	Fe (%)	4.55 ± 0.23	7.51 ± 0.28

3.1.2 Abiotic nutrient release

Dry deposition mode

After 48 h of contact in 0.2 µm filtered surface seawater, the Eyja ash released around five times more dFe than the Pata dust (Table 3A) and similar amounts of dSi. The dFe released by ash is twice higher than the dFe addition in the Fe treatment while the dSi released by both aerosols (maximum 0.3 µM) is eight times less than Si addition in the Si treatment. Both aerosols were not a significant source of NOx whereas only Eyja released significant DIP concentration (representing half of the +P treatment addition). Nutrient solubility was highest for P (Eyja), followed by Si then Fe. Solubility from dust was more than ten times higher for Si compared to ash and four times higher for Fe, while the released nutrient concentration was equal (dSi) or lower (dFe) (Table 3A), which can be explained by the difference in PC.

Wet deposition mode

With a 12.5-fold higher PC, the Eyja ash dissolved 8–10 times more dSi and DIP and 18 times more dFe than the Pata dust, while NOx release was similar for both aerosols (Table 3C). The solubility of all tested nutrients from Pata dust was higher relative to Eyja ash in ARW. Interestingly, the Si solubility of Pata dust was higher in SW (1.25 % and 0.21 % in SW and ARW, respectively) but similar in both matrices for Eyja (~0.12 %). In contrast, Fe solubility was similar for Pata in both matrices (~0.044 %) but significantly higher for the estimation of Eyja in ARW than in SW (0.051 % in ARW compared to 0.011 % in SW). The calculation might be over-estimated, which has however no implication for the bioassay experiments. The solubility of DIP for Eyja was higher in ARW compared to SW.

After the addition of 2 % of unfiltered ARW into abiotic 0.2-filtered SW, the final nutrient release by ash compared to dust after 48 h in SW was higher for dFe and DIP (Table 3B). Thus, final dFe and DIP concentrations after a wet compared to a dry deposition event were equal for Pata and higher for Eyja. On the other hand, the wet deposition of aerosols induced a significant decrease in dSi concentration, and a wet Pata deposition surprisingly decreased the SW NOx concentration (Table 3B). Thus, the aerosols are a source of dSi only in dry deposition mode and no source of NOx in our experiments.

Table 3: Means of N, P, Si and Fe release (concentration after the experiment minus initial ARW or SW concentrations) and solubility (% released from initial element content in aerosol) of dust and ash after 48h of contact in 0.2 µm filtered surface seawater for particle concentrations of 2 $mg.L^{-1}$ Pata dust and 25 $mg.L^{-1}$ Eyja ash in (A) dry deposition mode (means at the five station) in filtered SW and (B) in wet deposition mode (HNLC station 11 only). (C) Nutrient release and solubility after 1h of contact with artificial rainwater at station 11 for particle concentrations of 100 $mg.L^{-1}$ for Pata dust and 1250 $mg.L^{-1}$ for Eyja ash.

(A)	**Released concentration**	NOx, µM	DIP, µM	dSi, µM	dFe, nM
	Pata	n.s.	n.s.	0.2 ± 0.2 [a]	0.7 ± 0.6 [a]
	Eyja	n.s.	0.10 ± 0.05	0.3 ± 0.1 [a]	3.8 ± 1.6 [b]
	solubility	N, %	P, %	Si, %	Fe, %
	Pata	n.s.	n.s.	1.25 ± 0.52 [a]	0.041 ± 0.035 [a]
	Eyja	n.s.	6.8 ± 3.4	0.11 ± 0.05 [b]	0.011 ± 0.005 [b]
(B)	**Released concentration**	NOx, µM	DIP, µM	dSi, µM	dFe, nM
	Pata	-0.5 ± 0.0	n.s.	-2.2 ± 0.6 [a]	0.7 ± 0.3 [a]
	Eyja	n.s.	0.4 ± 0.0	-1.2 ± 0.3 [b]	9.0 ± 0.1 [b]
	solubility	N, %	P, %	Si, %	Fe, %
	Pata	< 0	n.s.	< 0	0.041 ± 0.017 [a]
	Eyja	n.s.	29.7 ± 2.2	< 0	0.027 ± 0.000 [a]
(C)	**Released concentration**	NOx, µM	DIP, µM	dSi, µM	dFe, nM
	Pata	0.15 ± 0.03 [a]	1.65 ± 0.05 [a]	1.92 ± 0.10 [a]	47.2 ± 0.9 [a]
	Eyja	0.11 ± 0.01 [a]	15.41 ± 0.60 [b]	15.41 ± 0.24 [b]	856.7 ± 35.4 [b] *
	solubility	N, %	P, %	Si, %	Fe, %
	Pata	2.18 ± 0.50 [a]	60.6 ± 1.8 [a]	0.21 ± 0.01 [a]	0.058 ± 0.001 [a]
	Eyja	0.38 ± 0.02 [b]	20.8 ± 0.8 [b]	0.13 ± 0.00 [b]	0.051 ± 0.002 [b] *

Note: Only the significant releases in nutrients (mean concentrations at 48h in the dust/ash treatments significantly different from means in the control at t0 p-val < 0.05) are shown; n.s. stands for 'not significant'. Means that are not significantly different between dust and ash treatment for each element are labelled with the same superscript letter *a* or *b* (p > 0.05). Negative dissolution values express a decrease of NOx or dSi in SW after ARW addition. * Fe release and solubility of ash in ARW are estimated according to Equation 7.

3.2 Initial conditions of the seawater samples

LNLC stations

The surface seawater at the studied stations had contrasted physico–chemical and biological features as shown in Table 4. Stations 2 and 16 are located in the warmer and saltier LNLC

region where surface seawater is characterized by low or undetectable concentrations of NOx and DIP associated with low phytoplanktonic biomass and primary production (PP). The average dSi concentrations were similar at both sites (~1.7 µM). At both LNLC stations, the molar NOx/DIP ratio is strongly lower than the Redfield ratio (16/1) (Redfield, 1934), indicating a potential N limitation of the phytoplanktonic activity at surface, while the high dSi/NOx ratio (> 20) indicates that Si is not the limiting nutrient in the LNLC region. The highest value of dFe relative to other stations is recorded at station 2 (0.54 nM), but this concentration remains low and Fe might be a co-limiting factor of primary production.

At both sites, the phytoplankton biomass was dominated by picophytoplankton (~63 % of Tchla) and nanophytoplankton (~26 % of Tchla). Moreover, prokaryotes were the main component of the picophytoplankton size class, as assessed by the high cyanobacteria-specific zeaxanthin concentration (~0.036 µg.L^{-1}). Biogenic Si was below detection limit at the LNLC stations, which is in good agreement with the very low diatom-specific fucoxanthin concentrations. The highest cellular abundance in the < 30 µm size-fraction is represented by *Synechococcus* cyanobacteria in the western LNLC station 2, but this genus was not detected at the eastern station 16. Likewise, no *Prochlorococcus* cells were detected by flow cytometry at any studied station, which will be discussed in section 4.1.

HN-LSi-LC station

South of the STF, station 14 lies within the HN-LSi-LC zone, and is characterized by colder and less salty surface waters, associated with a strong increase in NOx and DIP concentrations (Table 4), relieving potential N and P limitations. The dissolved Si concentration is the lowest (~1 µM) and consequently, the molar dSi/NOx ratio of 0.12 is well below the elementary ratio of 1.12 determined by Brzezinski (1985) for diatoms, suggesting a potential Si limitation of diatoms in this HN-LSi-LC area. As dFe concentration is low (0.39 nM), Fe may additionally limit phytoplankton growth.

The PP and algal biomass increased by a factor 7 to 12 compared to the LNLC region. The phytoplankton structure is modified: nano- and microphytoplankton dominate (respectively 54 and 28 % of Tchla) whereas picoplankton represents only 18 % of Tchla. At this station, the Tchla concentration is the second highest of the five sampled stations, while the pigments peridinin, 19'HF, alloxanthin and chlorophyll-b (biomarkers for dinoflagellates,

chromophytes/nanoflagellates, cryptophytes and chlorophytes, respectively) were the most abundant of all stations (data not shown). Based on pigment analysis, the nanoplankton biomass is largely dominated by nanoflagellates and chromophytes (99 % of the nanoplankton biomass), whereas microplankton biomass is comprised of 58 % dinoflagellates and 42 % diatoms (diatoms represented ~11 % of Tchla in agreement with the low bSi concentration). The highest cell abundances in the < 30 µm community are recorded at the HN-LSi-LC station 14 with an eight fold increase in *Synechococcus* and nanoeukaryote abundances and a 13 and 2-fold increase in picoeukaryotes and heterotrophic bacteria abundances respectively, relative to the LNLC stations.

451 **Table 4**: Initial physico-chemical and biological properties of the surface seawater used for the
452 microcosm experiments. Mean nutrient concentration ± standard deviation of replicates. DL =
453 detection limit. PP = primary production; bSi = biogenic silicon; Tchla = total Chlorophyll a.
454 Phytoplankton size-fractions according to Uitz et al. (2009): pico: 0.4-2 µm, nano: 2-10 µm,
455 micro: > 10 µm.

Station	**2**	**16**	**14**	**A3**	**11**
Zone	**STZ**	**STZ**	**SAZ**	**AZ**	**AZ**
Region	**LNLC**	**LNLC**	**HN-LSi-LC**	**Plateau**	**HNLC**
Latitude, degrees S	29.97	35.00	42.49	50.64	56.50
Longitude, degrees E	54.11	73.47	74.90	72.05	62.99
Sampling date	12 Jan 2019	05 Feb 2019	30 Jan 2019	27 Jan 2019	23 Jan 2019
Temperature, °C	24.6	22.0	12.8	4.4	2.1
Salinity	35.47	35.48	34.49	33.83	33.83
NOx, µM	< DL	< DL	8.11±0.41	20.60±0.77	25.25±0.01
DIP, µM	0.03±0.00	0.09±0.01	0.65±0.02	1.04±0.05	1.58±0.16
dSi, µM	1.79±0.05	1.61±0.05	0.99±0.00	1.59±0.06	16.67±0.15
NOx/DIP	< 2.7	< 0.9	12.5	19.8	16.0
dSi/NOx	> 22.4	> 20.1	0.12	0.08	0.67
dFe, nM	0.54±0.12	0.37	0.39	0.35±0.13	0.27±0.02
dMn, nM	1.17±0.05	0.72±0.02	0.30±0.01	0.14±0.03	0.24±0.02
dCo, pM	4.6±0.7	7.9±1.3	8.9±1.2	20.0±1.2	14.3±1.9
Synechococcus, cells.mL^{-1}	1 703	< DL	13 620	349	< DL
picoeukaryotes, cells.mL^{-1}	452	882	5 786	401	571
nanoeukaryotes, cells.mL^{-1}	339	209	2 798	644	1 176
heterotrophic bacteria, cells.mL^{-1}	655 782	547 742	1 310 728	615 636	441 028
PP, mg C.m^{-3}.d^{-1}	2.78	3.67	26.7	54.42	7.24
bSi, µmol.L^{-1}	< DL	< DL	0.11±0.02	2.31±0.79	0.96±0.48
Tchla, µg.L^{-1}	0.085	0.049	0.603	1.40	0.157
Fucoxanthin, µg.L^{-1}	0.004	0.002	0.046	0.688	0.047
Zeaxanthin, µg.L^{-1}	0.045	0.026	0.011	0.002	0.001
bSi/fucoxanthin, mol.g^{-1}	< 2.5	< 5	2.4	3.4	20.4
% micro	13	10	28	92	45
% nano	24	28	54	7	54
% pico	63	62	18	1	2

456 **HNLC and the plateau stations**

457 South of the PF within the AZ, SST and SSS at stations 11 and A3 were the lowest while NOx
458 and DIP reached maximum values (> 20 µM and > 1 µM, respectively). The Kerguelen plateau
459 station A3 and offshore HNLC station 11 are characterized by different dSi concentrations
460 leading to contrasting dSi/NOx ratios: the plateau station presents a potential Si limitation (dSi of
461 1.59 µM and dSi/NOx ratio of 0.08), whereas the offshore station 11 contains ten times more

462 dSi, raising the dSi/NOx ratio to 0.67, which is closer to the elementary compositional ratio of
463 diatoms (1.12 ± 0.33, Brzezinski, 1985). Moreover, Fe concentrations of respectively 0.35 and
464 0.27 nM may be limiting at both sites.
465 The highest PP and Tchla are recorded at the plateau station A3 (54.42 mg $C.m^{-3}.d^{-1}$ and 1.40
466 $\mu g.L^{-1}$). The phytoplankton community is considerably shifted with 92 % of Tchla composed by
467 microphytoplankton (> 20 µm). The diatom-specific pigment fucoxanthin is 15 times more
468 important than in the surrounding AZ (station 11) and SAZ (station 14). The second biomarker
469 for microphytoplankton, the dinoflagellate-specific pigment peridinin, is increased only by a
470 factor of five compared to the HNLC station 11, indicating that diatoms are the major contributor
471 of Tchla (diatoms contribute to 98 % of the chla biomass of the microplankton) at this fertilized
472 station. This result is consistent with literature data indicating similar high fucoxanthin and bSi
473 concentrations (Armand et al., 2008; Uitz et al., 2009).
474 The open HNLC station 11 holds eight and nine times less PP and Tchla than at the naturally Fe-
475 fertilized plateau station A3. The phytoplankton community structure is different compared to
476 the plateau, with twice less microplankton and six times more nanoplankton, contributing
477 respectively 45 and 54 % to the Tchla biomass. Picophytoplankton was negligible at both
478 stations with a contribution to Tchla lower than 2 %.

479 **3.3 Biological responses**

480 **3.3.1 Primary production**

481 At the LNLC stations 2 and 16, the addition of N and NP led to a significant increase in PP,
482 reaching a mean maximum relative change (RC, Eq. 8) of ~+150 % and ~+125 % at stations 2
483 and 16 respectively (Fig. 2a,b). No significant difference was observed between +N and +NP
484 treatments, indicating that the phytoplanktonic activity is mainly N limited. The addition of Fe
485 and Si, as well as the dust and ash additions promoted significantly and similarly PP only at the
486 western station 2 (~+65 %).
487 At the HN-LSi-LC station 14, additions of Fe and/or Si as well as dust triggered a similar and
488 significant increase in PP (~+35 %), while ash addition had two times more influence (+66 %,
489 Fig. 2c). Likewise, at station A3, both Fe and Si additions led to an increase in PP (~+80 %), and
490 FeSi triggered significantly more PP than Si, suggesting Fe and Si co-limitation (Fig. 2d). Of all
491 stations, aerosol additions at the plateau station A3 induced the highest PP increase (~+105 %).

At the HNLC station 11, the maximum increase in PP (~+80 %) is recorded after Fe addition. Aerosol additions in both dry and wet deposition modes stimulated PP (~+40 % on average, $p < 0.05$), and a dry deposition of ash had a significantly higher impact than a dry deposition of dust.

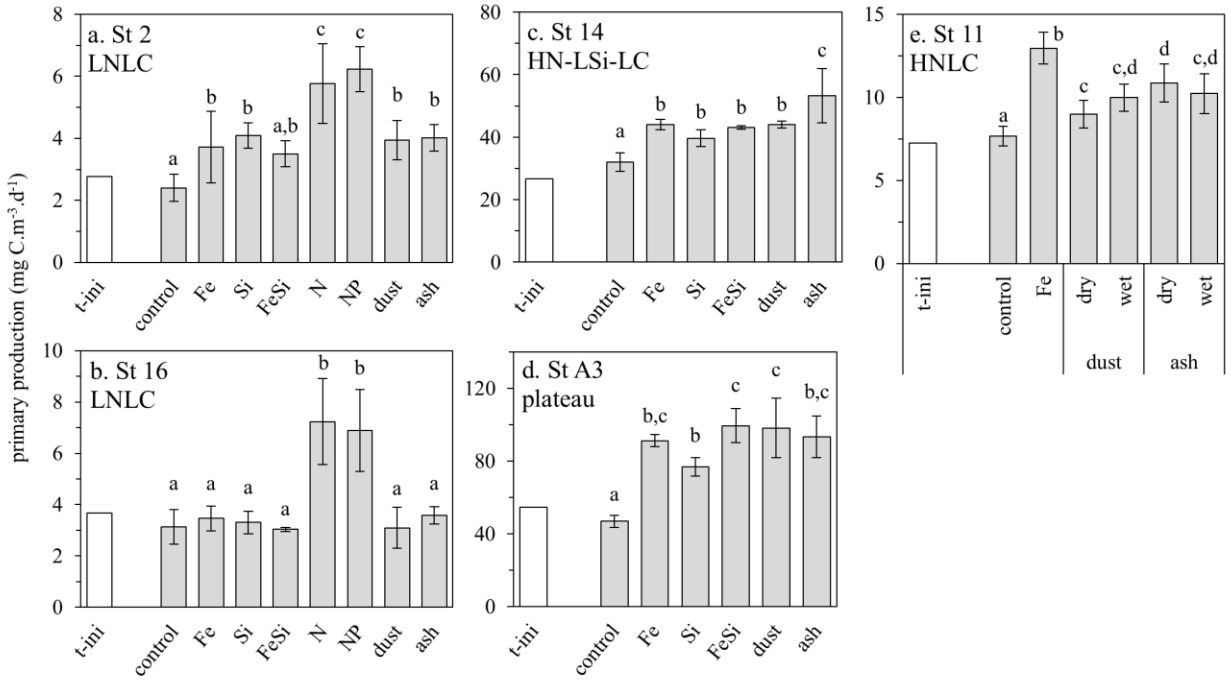

Figure 2. Primary production (PP, mg $C.m^{-3}.d^{-1}$) at the beginning of the experiment (t-ini, white bar) and after 48h of incubation for each treatment at the stations LNLC St 2 (a) and 16 (b), HN-LSi-LC St 14 (c), plateau St A3 (d) and HNLC St 11 (e). Error bars indicate standard deviation of triplicates. Means that are not significantly different are labelled with the same letter ($p > 0.05$) within a station.

3.3.2 Cellular abundances

At the western LNLC station 2, additions of Fe, FeSi, N and NP led to a similar stimulation of the picoeukaryote abundance (~+93 %, Fig. 3a). Si and NP additions induced the highest response of nanoeukaryote abundance (~+340 %, Fig. 3b) which was significantly different to that observed in Fe and N (~+220 %). On the contrary, *Synechococcus* abundance is just stimulated after N and NP additions (~+90 %, Fig. 3c). Aerosol addition had a different impact according to the phytoplankton type: picoeukaryotes were greater stimulated by dust (+96 %) than by ash addition (+50 %), while both aerosols had a similar effect on *Synechococcus* (~+70 %), and no effect on nanoeukaryotes. Surprisingly, at the eastern LNLC station 16, only the

addition of N and NP induced an increase in nanoeukaryote abundance (~+75 %) and ash stimulated picoeukaryote abundance by +38 % (Fig. 3d,e).

At the HN-LSi-LC station 14, none of the tested nutrients (Fe and/or Si) impacted the cell abundance of the assessed phytoplankton (< 30 µm). Only ash addition stimulated picoeukaryote abundance (+32 %, Fig. 3f), and dust enhanced nanoeukaryote abundance (+44 %, Fig. 3j), while no addition stimulated *Synechococcus*.

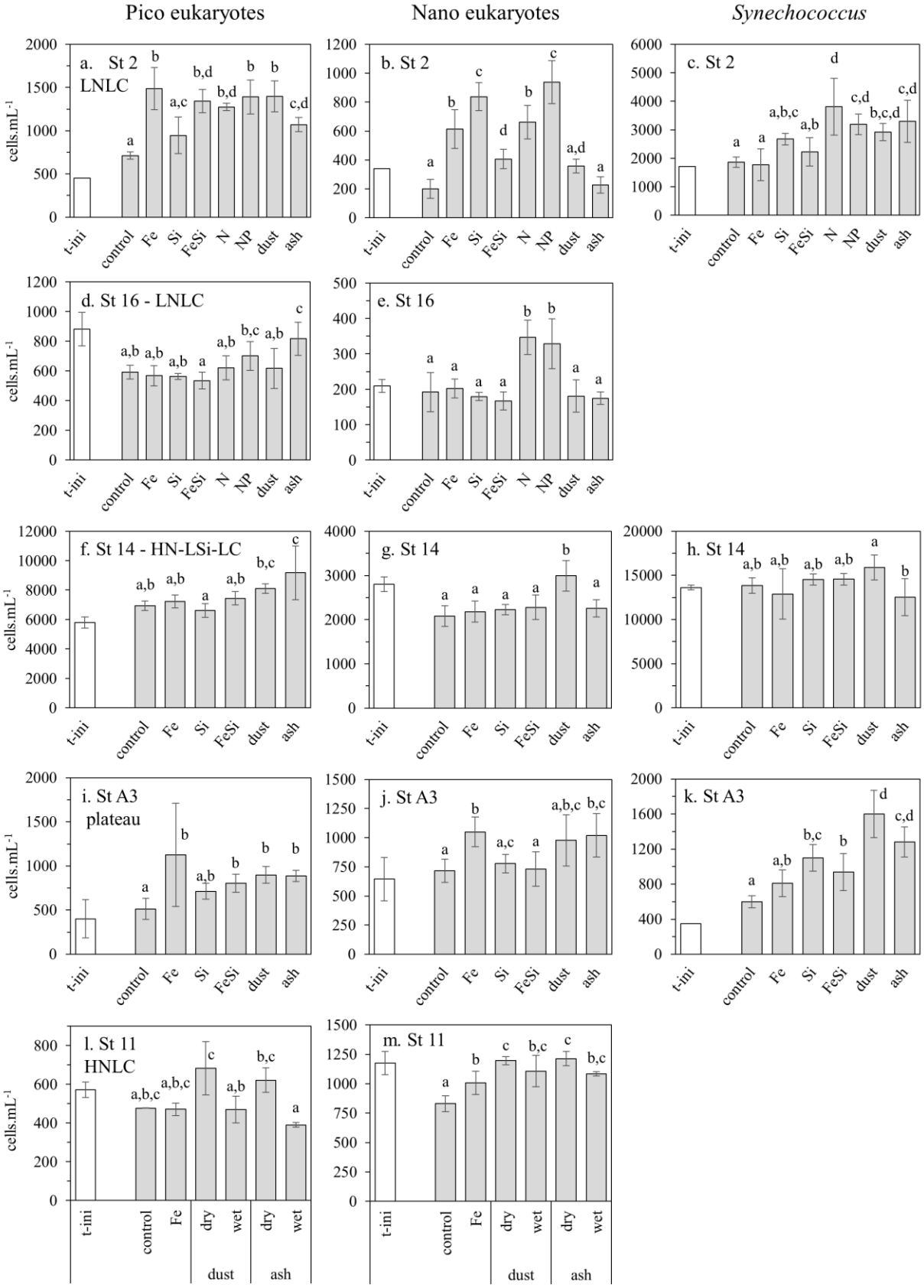
Pico eukaryotes
Nano eukaryotes
Synechococcus
a. St 2 LNLC
b. St 2
c. St 2
d. St 16 - LNLC
e. St 16
f. St 14 - HN-LSi-LC
g. St 14
h. St 14
i. St A3 plateau
j. St A3
k. St A3
l. St 11 HNLC
m. St 11
cells.mL-1
t-ini
control
Fe
Si
FeSi
N
NP
dust
ash
dry
wet

Figure 3. Cell abundance (cells.mL^{-1}) of pico eukaryotes (a,d,f,i,l), nano eukaryotes (b,e,g,j,m) and Synechococcus (c,h,k) at the beginning of the experiment (t-ini, white bar) and after 48h of incubation for each treatment at the LNLC St 2 (a-c) and 16 (d-e), HN-LSi-LC St 14 (f-h), plateau St A3 (i-k) and HNLC St 11 (l-m). Error bars indicate standard deviation of triplicates. Means that are not significantly different are labelled with the same letter ($p > 0.05$) within a station.

Contrariwise, at the Kerguelen plateau (station A3), Fe addition increased both pico- and nanoeukaryote abundances (+120 % and +50 % respectively, Fig. 3i,j). Surprisingly, Si or FeSi additions generated a *Synechococcus* development (~+70 %) that was not significant after Fe addition. +Dust and +ash triggered similar responses within a phytoplankton type, increasing cell abundance by 140, 75 and 40 % for *Synechococcus*, pico- and nanoeukaryotes respectively.

At the HNLC station 11, Fe addition increased just the nanoeukaryote abundance (+21 %, Fig. 3m). Wet and dry addition of dust or ash induced a similar stimulation of the nanoeukaryote abundance (~+40 %), whereas the effect on picoeukaryotes was not significant (Fig. 3l).

The abundance of heterotrophic bacteria (Fig. S1) increased significantly at the LNLC station 16 after FeSi and NP treatments (~+60 %), as well as after dust and Si additions at station 14 (~+30 %) or ash at A3 (+30 %).

3.3.3 Pigments

Both Fe and Si additions enhanced the Tchla and fucoxanthin concentrations relative to the controls at the three stations within the SAZ (St 14) and AZ (St 11 and A3, Fig. 4), indicating phytoplanktonic and especially diatom biomass stimulation. At the HN-LSi-LC station 14, Fe and Si additions generated a similar Tchla increase (~+40 %, Fig. 4a) but Si induced a higher fucoxanthin increase than Fe (+130 % and +50 % respectively, Fig. 4d). Thus, while the microplankton size fraction was initially dominated by dinoflagellates (as assessed by the peridinin/fucoxanthin ratio, data not shown), diatoms benefit more of nutrients and particularly Si addition. At the plateau station A3, the stimulation after both nutriment additions was similar (+65 % and ~+70 % for Tchla and fucoxanthin, Fig. 4b,e), whereas ash addition induced a higher increase in both pigments relative to the dust treatment (Fig. 4b,e). At the high and low Si HNLC stations (11 and 14), no significant difference for both pigments was noted after a dry addition of dust and ash: we observed a Tchla increase of ~+60 % at both stations, while fucoxanthin increase was higher at the low-Si station 14 compared to the high-Si station 11 (~+115 % and

548 ~50 %, respectively). Moreover, a wet deposition of ash at the HNLC station 11 had a twice
549 lower impact on Tchla increase than a dry deposition (+37 % and +74 %, respectively). The
550 contribution of different size fractions to Tchla increase will be further discussed in section 4.2.

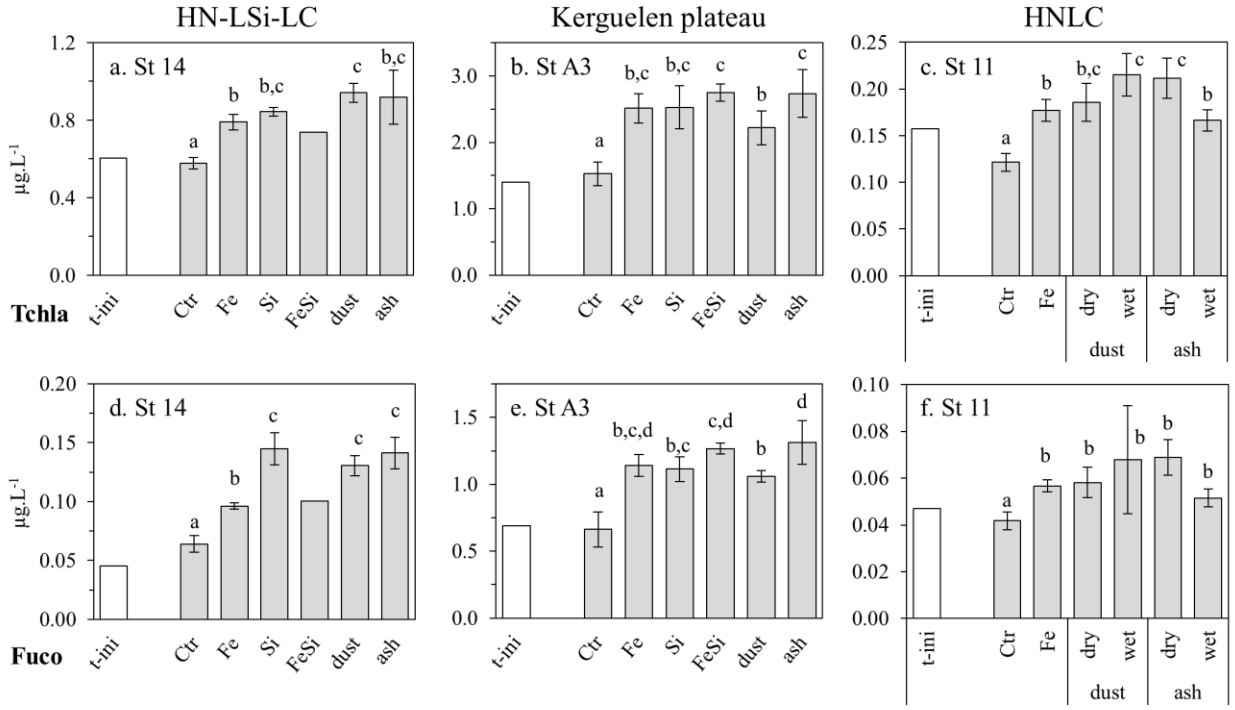

551
552 **Figure 4**: Pigment concentration (µg.L^{-1}) of total Chlorophyll-a (a-c) and fucoxanthin (d-f) at the
553 beginning of the experiment (t-ini, white bar) and after 48h of incubation for each treatment at
554 HN-LSi-LC St 14 (a,d), plateau St A3 (b,e) and HNLC St 11 (c,f). Error bars indicate standard
555 deviation of triplicates. FeSi treatment at St 14 is not included in statistics, due to n = 1. Means
556 that are not significantly different are labeled with the same letter ($p > 0.05$) within a station.

557 3.3.4 Biogenic silicon

558 Both Si and FeSi additions strongly enhanced the bSi concentration at the HN-LSi-LC station 14,
559 (+100 % and +60 %, respectively, Fig. 5a) whereas an addition of Fe had no impact. The
560 Kerguelen plateau station A3 and HNLC station 11 were both diatom-dominated and the bSi
561 concentration was high (around 3.0 and 2.0 µmol.L^{-1} respectively, Fig. 5b,c), but no influence of
562 the nutrient treatments was observed.

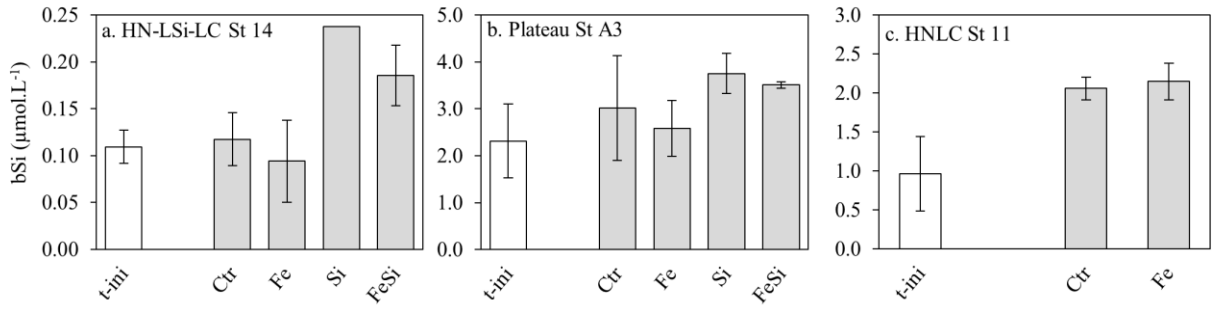

Figure 5: Biogenic silica concentration (bSi, µmol.L^{-1}) at the beginning of the experiment (t-ini, white bar) and after 48h of incubation for each nutrient treatment at the HN-LSi-LC St 14 (a), plateau St A3 (b) and HNLC St 11 (c). Error bars indicate the range from duplicates besides Si treatment at St 14 (with n = 1).

4 Discussion

4.1 Initial conditions and ambient nutrient limitations

The progressive shift from the oligotrophic gyre of the SIO towards the macronutrient-rich SO is associated with a shift in the phytoplankton community. Thus, the warm LNLC waters of the SIO are dominated by picoplankton which decline with decreasing SST, whereas microplankton increases and becomes the main size class in the SO. Relative nanoplankton proportion is maximal in the HN-LSi-LC region within the SAZ (Table 4, Fig. 7).

A recent publication based on cruise data from the same study zone focused on the community composition shaped by hydrographic fronts of the SIO and SO (Hörstmann et al., 2021). The authors were the first to measure PP in the western SIO and in different regions of the Indian SO, and their results on productivity and pigment signature are in good agreement with our findings for initial conditions in the LNLC, HN-LSi-LC and HNLC zones.

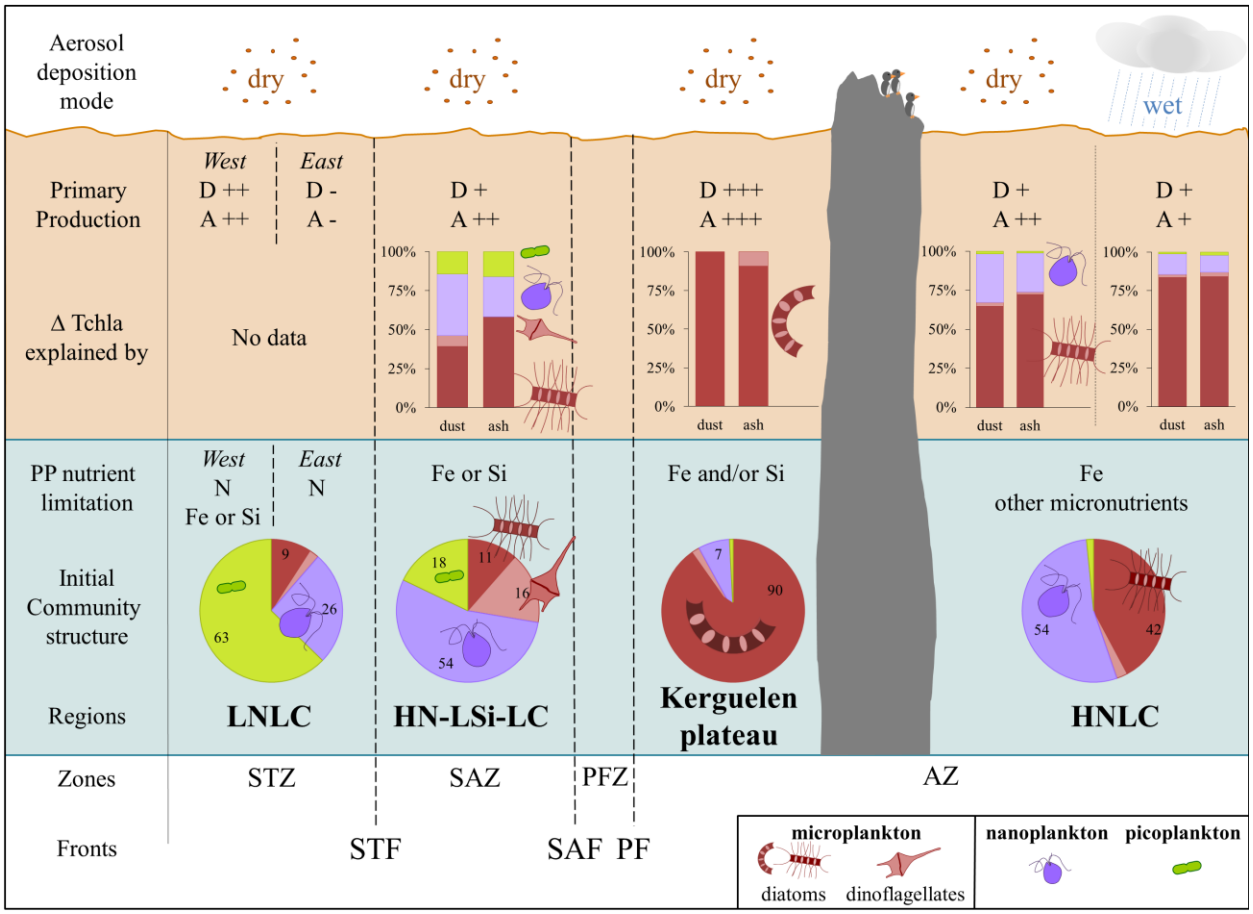

Figure 6. Schematic representation of the biological response of phytoplankton communities after dry or wet dust (D) and ash (A) deposition to the sea surface within different biogeochemical regions of the South Indian Ocean and Southern Ocean. The top part of the figure (orange box) shows the phytoplankton response to aerosol deposition (PP and ΔTchla), while the bottom part (blue box) represents the initial conditions prior to deposition (nutrient limitation and phytoplankton structure). Primary production is expressed in relative change (%), as follows: +++ above 100%; ++ above 50%; + below 50%; − no significant change compared to control. ΔTchla shows the contribution (%) of different phytoplankton classes explaining the global increase in Tchla. The community composition (initial and final) is based on the pigment signature, with red: microplankton (dark: diatoms and light: dinoflagellates), purple: nanoplankton and green: picoplankton. The schema concerns solely the surface layer and response after 48h, regardless of depth and particle sinking. The represented taxa are representative for the SO: microplankton: *Eucampia* and *Chaetoceros* (coastal and open ocean diatoms, respectively), *Ceratium* (dinoflagellate); nanoplankton: *Phaeocystis* (haptophyte); pico-plankton: *Synechococcus* (cyanobacteria). Zones and fronts (from North to South): Subtropical Zone and Front (STZ and STF), Subantarctic Zone and Front (SAZ and SAF), Polar Front Zone and Front (PFZ and PF) and Antarctic Zone (AZ).

598 **LNLC stations**

599 The SIO remains one of the least known ocean regions due to under-sampling relative to other
600 regions like the North Atlantic and Tropical Pacific oceans. Its NOx and DIP depleted surface
601 waters associated with low phytoplankton biomass and productivity are confirmed by previous
602 studies (Estrada et al., 2016; Hörstmann et al., 2021; Thomalla et al., 2011; Wiggert et al., 2006).
603 Recently, Twining et al. (2019) measured surface dFe of 0.2 nM and nitrate concentration below
604 0.05 µM and identified N limitations in the Eastern SIO dominated by *Prochlorococcus*, whereas
605 Browning et al. (2017) investigated the impact of Co additions in the Eastern South Atlantic
606 Ocean gyre and determined N-Fe-Co co-limitations. Their limiting concentrations of 0.014-1.833
607 µM NOx, 0.09-0.37 nM dFe and 0.01-0.02 nM dCo are similar to the initial nutrient conditions
608 in our LNLC study zone (Table 4) and indicate that the phytoplankton community could also be
609 co-limited by micronutrients such as Fe or Co in addition to N limitation.
610 It is to be noted that the eastern station 16 was sampled three weeks after the western station 2
611 (Table 4), which might have affected the local nutrient dynamics as well as the phytoplankton
612 community structure and response, despite a generally low seasonality within the STZ.
613 Moreover, Figure 1a displays the potential influence of the South East Madagascar Bloom
614 (SEMB) at the western station 2 that might explain higher initial algal biomass, whereas station
615 16 lays in more typical oligotrophic waters.
616 In our study in the Western part of the SIO, the phytoplankton composition was dominated by
617 the picoplankton size fraction, and the relative *Synechococcus* and picoeukaryotes abundances of
618 the western LNLC station 2 (54.11° E) are in good agreement with published data from LNLC
619 stations around 59° E and 70° E (Agusti et al., 2019; Liu et al., 2019). To our knowledge, the
620 absence of *Synechococcus* at our eastern LNLC station 16 (73.47° E) is documented for the first
621 time. Although Agusti et al. (2019) identified *Prochlorococcus* cells in the surface waters within
622 the study zone, the non-detection of the prochlorophytes in the STZ in our study is confirmed by
623 data collected in the same area during the SOCLIM cruise (Liu et al., 2019) as well as by recent
624 measurements during the SWINGS cruise (Obernosterer, pers. com., 2021). The prochlorophyte-
625 specific pigment divinyl-chlorophyll-a was however detected at both LNLC stations in our study
626 (16–30 $ng.L^{-1}$ divinyl-chlorophyll a), whereas the divinyl-chlorophyll b was close to the
627 detection limit (~1 $ng.L^{-1}$). The presence of such *Prochlorococcus*-specific pigments without
628 cytometric detection might be an indication that the fluorescence of the cells was too low to be

detected by flow cytometry. Indeed, the cellular photosynthetic pigments of *Prochlorococcus* are strongly reduced when the cells are exposed to high light in surface waters. Another hypothesis states that the *Prochlorococcus cells* may not be free-living, but could occur as aggregates (Cruz and Neuer, 2019), and therefore, would remain undetected by flow cytometry.

HN-LSi-LC station

The general nutrient limitations of the low and high Si HNLC areas of the Indian SO are well known and have been monitored in the context of C cycling and associated air–sea CO_2 fluxes within the framework of the OISO program (Jabaud-Jan et al., 2004; Metzl et al., 2006). Dissolved Fe and dSi concentrations of 0.29 nM and 0.5 µM respectively have been assessed at the confluence of the Western Indian SAZ and STF at ~63° E off the coast of Crozet Island (Blain et al., 2002; Sedwick et al., 2002), whereas Grand et al. (2015a) report 0.18 ± 0.10 nM dFe in the surface SAZ of the central SIO at 95° E. These concentrations are slightly lower but comparable to our study site at 75° E (0.39 nM dFe and 0.99 µM dSi, Table 4). Several bottle incubation studies concluded on phytoplankton FeSi co-limitation in the Indian (Sedwick et al., 2002) and Australian (Hutchins et al., 2001) sectors of the SAZ.

Also in the Australian SO, Fripiat et al. (2011b) estimated a net loss of bSi production in the Australian summer SAZ and observed similar bSi concentrations (0.1 $\mu mol.L^{-1}$) to our measurements. In our study, the relative low bSi/fucoxanthin ratio of 2.4 $mol.g^{-1}$ indicates that the diatoms are lightly silicified. However, surface phytoplankton community and productivity records remain scarce in the SIO and Indian SO.

HNLC and the plateau stations

The dFe concentrations of the SO stations in this study (0.35 nM at the plateau station A3 and 0.27 nM at the HNLC station 11) were higher compared to data found by Blain et al. (2008) during the same period of the year in the austral summer (KEOPS-1, January–February 2005). These authors measured 0.090 ± 0.034 nM dFe in the surface ocean at the Kerguelen plateau reference station A3 and 0.073 ± 0.014 nM dFe within the surrounding HNLC zone, whereas our dFe concentration at A3 was more comparable to the 0.3-0.4 nM measured during the austral spring (KEOPS-2, October–November 2011) (Bowie et al., 2015). Grand et al. (2015a) reported 0.34 ± 0.15 nM dFe in the surface AZ of the Indian SO around 82° E. In the Atlantic sector of

658 the SO however, Chever et al. (2010) and Trimborn et al. (2017) measured surface dFe
659 concentration of ~0.25 nM which are more comparable to our concentrations, whilst remaining
660 characteristic for Fe-limitation, as demonstrated by their photosynthetic efficiency
661 measurements.
662 Other parameters such as pigments and bSi concentrations at the plateau station A3 were in good
663 agreement with the literature (Armand et al., 2008; Uitz et al., 2009). For instance, the
664 bSi/fucoxanthin ratio of living cells of 4.9 ± 1.0 mol.g^{-1} recorded by Mosseri et al. (2008) during
665 the KEOPS1 cruise for the same station is close to our ratio of 3.4 mol.g^{-1}. Moreover, the low dSi
666 concentration at A3 (10.5 times lower than at the HNLC station 11) and the season in late
667 summer (end of January) are indicators that the plateau ecosystem is close to Si limitation at the
668 end of the diatom bloom.
669 Further, while the fucoxanthin signature of the low and high Si HNLC stations (14 and 11) are
670 comparable (0.047 µg.L^{-1}), the bSi content of the HNLC station 11 is nine times higher than at
671 the HN-LSi-LC station 14, inducing a 8.5-times higher bSi/fucoxanthin ratio of 20.43 mol.g^{-1}.
672 This ratio is comparable to other HNLC stations of the SO (18.2 ± 2.7 mol.g^{-1} of living cells,
673 Mosseri et al., 2008) and indicates heavily silicified diatoms which may be explained by Fe
674 limitation (Claquin et al., 2002; Nunn et al., 2013).

675 **4.2 Phytoplankton response to aerosol additions**

676 The abiotic experiments performed within the scope of this study (Table 3) demonstrated that the
677 tested Pata dust and Eyja ash released significant amounts of Fe and Si to seawater. However,
678 neither the dust nor the ash particles were a significant source of NOx to SW, as shown in Table
679 3. This is also consistent with previous results using Saharan dust (Mills et al., 2004; Ridame et
680 al., 2014) and ash (Browning et al., 2014; Jones and Gislason, 2008). Thus, dust and ash addition
681 possibly relieved or reduced Fe and/or Si limitations of the SO but not the regional N limitation
682 of the SIO. The main phytoplankton response to aerosol additions is synthesized in Figure 6.
683 Possible Fe contamination of the +Si treatment is thought to be negligible for general
684 conclusions (see discussion in Supplementary Material S1).

LNLC stations

While the PP increases at the eastern station 16 after N additions could be explained at least by an increase of nanoeukaryote abundance (Fig. 2b and 3e), the response pattern is more complex at the western LNLC station 2, where phytoplankton groups responded differently to the nutrients released by aerosols. Dust and ash stimulated significantly picoeukaryotes and *Synechococcus* but not nanoeukaryotes, whereas Fe stimulated pico- and nanoeukaryotes but not *Synechococcus*, and Si triggered solely nanoeukaryotes response, suggesting the presence of nano-sized (< 30 µm) diatoms or other Si-requiring species such as silicoflagellates (Shetye et al., 2014; Shiro, 1986). For the LNLC stations, we could not analyze pigment content at the end of the 48 h experiment, hindering a more precise identification of the responding phytoplankton group.

The difference between aerosols compared to nutrients might be the release of other micronutrients such as Co that was released significantly to the SW in the abiotic Pata and Eyja experiments (data not shown). It is to be noted that FeSi and NP additions stimulate heterotrophic bacteria at the eastern LNLC station (St 16, Fig. S1b), which may compete for nutrient uptake and limit autotroph response, as observed in the oligotrophic tropical Atlantic (Marañón et al., 2010).

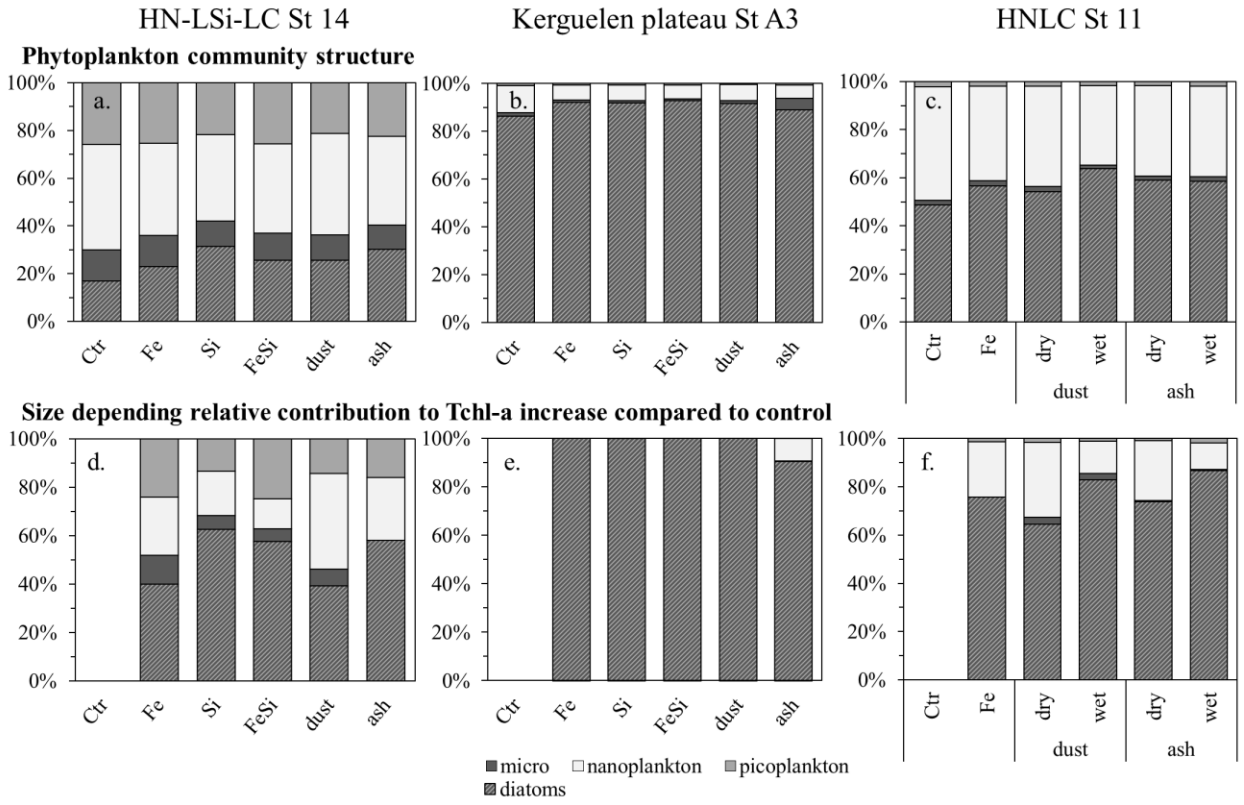

Figure 7. Phytoplankton community composition (%, a-c) with relative abundances of micro- (dark), nano- (light) and pico-phytoplankton (median grey) calculated from pigment analysis according to equations 3 and 4, and contribution (%, d-f) of different size fractions to the increase in Tchla after 48h of incubation for each treatment relative to control (equation 5), at the HN-LSi-LC St 14 (a,d), plateau St A3 (b,e) and HNLC St 11 (c,f). Diatom contribution within the micro-plankton size fraction is dashed.

HN-LSi-LC station

At the HN-LSi-LC station 14**,** PP is mainly stimulated by ash addition. The microplankton contribution to the total biomass (expressed as Tchla, Fig. 7a) increases after nutrient or aerosol addition (initial 28 %, and reaching up to 36 and 42 % after Fe and Si additions, respectively). Moreover, the increase in Tchla relative to the control (~+46 %, Fig. 4a) is mainly caused by the micro size fraction (Fig. 7d), but nano- and picophytoplankton also benefit from the nutrient/aerosol addition. Hence, the Tchla increase is explained for 58 %, 25 % and 17 % by respectively micro, nano- and picophytoplankton biomass increase (Fig. 7d), independent of the treatment. Diatoms benefit particularly from the nutrient supply, since their contribution to the phytoplankton community increases from only 17 % in the control assemblage up to 30 % after ash or Si additions (Fig. 7a). Thus, the diatom development alone is sufficient to explain an

720 average 51 % of the total Tchla increase (Fig. 7d), whereas the contribution of dinoflagellates to
721 the Tchla increase averages to only 7 %. The dominance of the diatom response to Fe and/or Si
722 additions compared to that of dinoflagellates has also been reported for the Australian SAZ
723 (Hutchins et al., 2001).
724 Monitored by the increase in fucoxanthin concentration, diatoms responded equally to dust, ash
725 and Si additions (~+120 %, Fig. 4d), indicating that the diatom Si-limitation may be alleviated by
726 the aerosol input. In the abiotic experiment, a dry deposition of dust or ash released around 0.3
727 µM dSi (Table 3A), which indicates that the initial Si-limitation could be eased with a relatively
728 low absolute release representing +20 to +33% of the initial stock (initial dSi concentration of
729 0.99 µM; Table 4). The increase in bSi concentrations after Si and FeSi additions confirms the
730 increased development and/or silicification of diatoms at the HN-LSi-LC station (Fig. 5a).
731 The pico- and nanoeukaryote cell abundances responded significantly to ash and dust additions
732 (32 % and 44 %, respectively, Fig. 3f,g), but not to Fe and/or Si. This result indicates that pico-
733 and nanoeukaryotes growth may be limited by other micronutrients that were released from the
734 aerosols, for example Co, as already mentioned for LNLC stations, or Mn (Fishwick et al.,
735 2018). Alternatively, pico- and nanoeukaryotes may be less competitive than diatoms for new
736 nutrient uptake. The *Synechococcus* abundance was the highest recorded during the cruise but
737 did not evolve after new nutrient supply, indicating that this species was not nutrient-limited in
738 local conditions, could not benefit from this addition and/or were subjected to important grazing.
739 Hutchins et al. (2001) performed a similar trace metal clean bottle experiment involving Fe
740 and/or Si additions in the SAZ of the Australian sector of the SO. Comparable to our results, the
741 authors observed Fe and Si co-limitation of diatoms but no impact of the treatments compared to
742 the control for cyanobacteria, described as mostly *Synechococcus*.

743 **HNLC station**

744 Similar to Fe addition, dust and ash input led to a stimulation of PP and Tchla, confirming that
745 dry and wet depositions of dust and ash are a significant source of bioavailable Fe for
746 phytoplankton, as assessed in the abiotic experiment (Table 3) and as previously shown in
747 several HNLC areas of the ocean (Langmann et al., 2010b; Mélançon et al., 2014, 2016;
748 Trimborn et al., 2017). The increase in Tchla after direct or atmospheric Fe addition in the
749 HNLC zone was mainly generated by the increase of the microplankton biomass (representing

~78 % of the Tchla increase, Fig. 7f) and in particular by the diatom biomass increase that sustained over 95 % of the microplankton biomass increase (Fig. 7f). Nanoplankton (nanoflagellates and chromophytes) took also part in the Tchla increase, with a contribution of about 20 %, in agreement with the increase in the nanoeukaryote abundances. The picoplankton contribution to Tchla increase was negligible (~1 %, Fig. 7f), confirmed by the absence of significant picoeukaryote abundance response to neither direct nor atmospheric Fe addition (Fig. 3l). As a result, the proportion of microplankton within the phytoplanktonic community slightly increased (~60 % compared to 51 % in the control community, Fig. 7c) at the expense of nanoplankton (~38 % compared to 47 %). Therefore, at the HNLC station, microplankton, and almost exclusively diatoms, are not only the main components of the phytoplankton community, but also the main beneficiaries of new nutrient release (Fig. 7f).

While PP is mostly stimulated by Fe addition, the responding phytoplankton groups are equally or more intensely stimulated by aerosols compared to Fe addition, indicating that both tested aerosols dissolve sufficient Fe in both dry and wet deposition modes to relieve the Fe-limitation of the HNLC region. Similarly, Browning et al. (2014) recorded a significant biological response after various ash and Fe additions in their bottle experiments in the West Atlantic sector of the SO. In contrast, Trimborn et al. (2017) performed similar dust and Fe addition incubation experiments in the Atlantic sector of the SO but using four times lower Fe concentrations (0.5 nM) and eight times lower dust input (0.25 $mg.L^{-1}$) than in our experiments. They did not record an increase in diatom growth rate after their low Fe addition, or a shift of the diatom-dominated phytoplankton community under actual CO_2 levels, which suggests that phytoplankton from the severely Fe-limited SO need a certain Fe threshold to be able to respond to a stimulation (Boyd et al., 2010).

Plateau station

At the Kerguelen plateau station A3, aerosol additions triggered a PP increase on par with that observed with the Fe and/or Si additions, indicating a Fe and Si growth limitation. Likewise to the HNLC station, the microplankton size fraction and more specifically diatoms constitute the main contributor to the phytoplankton biomass (92 %, of which 98 % are diatoms, Fig. 7b), as already observed by Uitz et al. (2009). Diatoms are sufficient to explain the entire Tchla increase observed after nutrient or aerosol additions (Fig. 7e). Timmermans et al. (2008) tested the impact

of naturally Fe- and Si-rich SW on the growth of the natural Kerguelen and open-ocean HNLC phytoplankton communities as well as on diatoms in monocultures during translocation experiments. The authors found that microphytoplankton, mainly diatoms, was responsible for the increased CO_2 assimilation, confirming the Fe (and/or Si) limitation on the Kerguelen plateau at the end of the diatom bloom. Silicon limitation at this season was also reported at A3 to explain the modeled annual evolution of the Si biogeochemical cycle (Closset et al., 2014). Even if the relative role of the < 30 µm community to Tchla increase remains insignificant compared to the dominating diatoms, it responded to the aerosol or nutrient additions at the plateau station: pico- and nanoeukaryotes increased their abundance after direct Fe addition and aerosols, whereas *Synechococcus* responded to aerosol inputs but also to Si addition. Silicon is not a common nutrient for cyanobacteria, but Si bioaccumulation within picocyanobacteria such as *Synechococcus* has already been observed in the western Pacific and Sargasso Sea as well as in cultured strains (Baines et al., 2012; Krause et al., 2017; Wei et al., 2021). However, such silicifying *Synechococcus* have not yet been detected near Kerguelen Islands to our knowledge.

The area over the Kerguelen Plateau was the most productive station (initial PP of 54.42 mg $C.m^{-3}.d^{-1}$; Table 4) and also the most responsive to nutrient or aerosol addition, with a mean 100 % PP increase (Fig. 2d). On the other hand, a lower relative response of PP was measured at the HNLC station (+~46 %). This variability in the biological response between the plateau and surrounding open ocean populations could be explained by a precondition of the Kerguelen phytoplankton community to frequent nutrient supply through winter mixing, accelerating the response to aerosol addition. The HNLC population is acclimated to Fe limiting concentrations, and it may require a longer period of time to reach maximal biological response. Thus, the experimental duration of 48 h may not have been sufficient to overcome the lag phase, as described by Moore et al. (2007) during the CROZEX *in situ* Fe addition experiment in the same sector of the SO, where the biological response occurred mostly after three days of incubation. Similarly, Timmermans et al. (2008) observed a twice longer lag phase (12 versus 6 days) in their HNLC phytoplankton experiment compared to the Kerguelen plateau phytoplankton community during translocation experiments.

808 ### 4.3 Influence of physico–chemical parameters on nutrient release

809 At each station, the addition of aerosols had either an enhancing or no impact on phytoplankton
810 since we never observed a net decrease in PP or any of the stocks at any station. Therefore the
811 stimulation after nutrient release has an equal or greater positive impact compared to a possible
812 inhibition effect due to the release of toxic elements (Paytan et al., 2009) as observed *e.g.* for Cu
813 release by European aerosols in the LNLC area of the Western Mediterranean Sea (Jordi et al.,
814 2012).

815 #### 4.3.1 Aerosol type: importance of origin and mineralogy

816 We tested the impact of two contrasting types of aerosols on the biological response of
817 phytoplankton. We compared representative depositions from a South American desert dust to
818 the ash emissions of an Icelandic stratovolcano. The Fe release by desert dust (Guieu et al., 2002;
819 Paris et al., 2011) and volcanic ash (Ayris and Delmelle, 2012; Duggen et al., 2007; Jones and
820 Gislason, 2008; Langmann et al., 2010b) has already been demonstrated, as well as their
821 bioavailability for phytoplankton (Hoffmann et al., 2012; Jacq, 2014). Despite a 12.5-fold higher
822 PC for the volcanic ash experiments (accompanied by a 5.4-fold higher abiotic dFe and similar
823 dSi release relative to dust, Table 3A), the biological response after a dry deposition of these
824 contrasted aerosols was overall similar; independently of the tested biogeochemical area or the
825 phytoplankton size class. The aerosols have a different mineral composition, as the ash is
826 dominated by a glassy (amorphous) constituent (Table 2). Aluminosilicate glass dissolves faster
827 than its crystalline counterpart (Wolff-Boenisch et al., 2006) and may be responsible for the
828 majority of Si release upon dissolution from ash (Morin et al., 2015). In contrast, the Si released
829 from desert dust likely originates from crystalline minerals' dissolution such as quartz, clays and
830 feldspar (Chou and Wollast, 1985; Wollast and Chou, 1988). In our experiment, we observed
831 identical Si release despite different PC, explained by significantly higher Si solubility of dust
832 (Table 3A).
833 The desert dust sample contained almost twice less Fe (4.55 % vs 7.51 %) than ash but twice
834 more clay minerals, well known for their role in Fe release (Journet et al., 2008). The smaller
835 particle size and specially the higher SSA of desert dust particles may also explain the four times
836 higher Fe solubility of dust relative to ash (Baker and Jickells, 2006). Iron solubility of dust

837 compared to ash is four times higher, indicating that the higher nutrient release from ash is
838 merely due to the higher PC.
839 At the LNLC station 2 and the Kerguelen plateau station A3, the PP increase was independent of
840 the aerosol type. At these stations, no significant difference in PP was visible between dust, ash
841 and Fe additions, suggesting that the Fe released by aerosols might be bioavailable and sufficient
842 to relieve the local Fe-limitation. It is plausible that the Fe-limitation was not very severe at these
843 stations and that the mean 0.7 nM dFe provided by the dust deposition was sufficient to reach the
844 maximal response rate of cell division and PP. A similar conclusion was drawn by Mélançon et
845 al. (2014), who performed ash addition bottle experiments with a concentration gradient in the
846 northeast subarctic Pacific Ocean. The authors observed a significant increase in absolute C
847 uptake and Chla specific productivity between low and medium ash concentrations of 0.12 and
848 1.2 $mg.L^{-1}$, respectively. Further, the biological response reached the characteristic plateau of a
849 hyperbolic Monod curve for their high PC (10 $mg.L^{-1}$), demonstrating that the phytoplankton did
850 not respond to nutrients in excess in the case of their six day incubation. A similar observation
851 was made by Browning et al. (2014) with a ten-fold increase in PC of the same ash sample and
852 similar biological response. Thus, we can conclude that the local phytoplankton communities
853 reached the plateau of the Monod curve concerning Fe after the addition of Fe or aerosols, but
854 may nonetheless be limited by N at the LNLC station.
855 On the other hand, at the HNLC stations 14 and 11 (with respectively low and high Si
856 concentration), a dry deposition of ash triggered around twice more PP than dust ($p < 0.05$). At
857 the HN-LSi-LC station 14, ash addition generated more PP than the nutrients Fe and/or Si, which
858 may be a sign that the ash released other limiting micronutrients (Frogner et al., 2001; Hoffmann
859 et al., 2012). However, it is unlikely that the Fe limitation was not completely resolved after Fe
860 addition, as the release of 2 nM Fe is meant to be in excess. At the HNLC station 11, Fe addition
861 induced more PP increase than aerosols, which suggests that unknown synergistic effects
862 between the released elements could weaken the positive effect of Fe release (Hoffmann et al.,
863 2012; Paytan et al., 2009) or that the local communities were differently influenced by the direct
864 nutrient supply of the Fe solution compared to the potentially more gradual nutrient dissolution
865 from the aerosols.

4.3.2 Deposition mode

The addition of desert dust and volcanic ash in both dry and wet deposition modes performed at the HNLC station 11 enabled direct comparison of the influence of ambient pH of the first contact medium (8.1 for seawater and 4.7 for rainwater) as well as the ionic charge and presence of organic matter found in SW. Indeed, Fe dissolution of dust particles is known to decrease with increasing pH (Desboeufs et al., 1999; Journet et al., 2008; Marcotte et al., 2020; Paris et al., 2011), whereas organic matter, and more precisely the presence of Fe binding ligands, increases Fe solubility and bioavailability in SW (Hassler et al., 2011; Paris and Desboeufs, 2013; Wagener et al., 2008), demonstrating the complexity of opposing controls impacting nutrient release.

In our abiotic control experience, the highest Fe solubilities for both dust and ash occurred in the ARW matrix (Table 3C). Moreover, while the deposition mode did not significantly influence the dFe release from dust to SW (0.7 nM after 48 h of contact, Table 3A,B), ash released 2.4 times more Fe to SW in wet compared to dry deposition mode (9.0 and 3.8 nM, respectively). The addition of 2 % ARW to SW should theoretically release 0.94 and 17.1 nM dFe to SW after wet dust or ash deposition. The difference between the measured wet deposition and theoretical release (significant only for ash deposition) may indicate that Fe adsorption and/or precipitation processes dominate over secondary Fe dissolution in the SW. Moreover, the quality and quantity of organic matter in the SW may explain the high variability in Fe solubility, as previously demonstrated (Bressac and Guieu, 2013; Wagener et al., 2008).

A wet deposition of either aerosol induced a moderate increase in PP (~+40 %, Fig. 2e), intermediate between the higher impact of dry ash deposition (+50 %) and a lower reaction after a dry dust deposition (+24 %). Equally, Tchla and fucoxanthin increases are independent of the dust deposition mode, consistent with the equal abiotic Fe dissolution (0.7 nM dFe), indicating that the Fe released by both mechanisms is equally bioavailable.

However, the dry deposition of ash triggered significantly more Tchla than the wet deposition (+74 vs. +37 % respectively, Fig. 4c). Although the response of the dominant diatoms did not vary between dry and wet deposition (Fig. 4f), other phytoplankton groups responded differently depending on the deposition mode. For instance, picoeukaryote abundance increased only when the dust or the ash was dry deposited (Fig. 3l), and the nanoplankton-size fraction (mainly the

haptophyte *Phaeocystis*, assessed by their 19'HF pigment signature, Fig. S2c) responded negatively to a wet deposition, despite a higher Fe release.

5 Conclusions

Our results from incubation experiments demonstrate that both tested aerosols of contrasting geographical, mineralogical and petrological characteristics released significant amounts of Fe and Si to seawater in the Indian and Southern Oceans. A schematic summary of our main results is presented in Figure 6. A representative deposition of both dust and ash was sufficient to trigger a biological phytoplankton response, mainly driven by a stimulation of the diatom community. The higher loading of ash compared to dust (2 and 25 $mg.L^{-1}$ for Pata dust and Eyja ash, respectively) probably explains the greater Fe release from the former, *i.e.* Fe content and solubility do not explain this result. Ash addition elicited an equivalent or greater biological response than the dust, depending on the severity of the initial Fe-limitation. Nevertheless, neither the tested Pata dust nor the Eyja ash was a source of NOx.

After dust or ash additions, the maximum relative and absolute PP increase was observed at the most productive station over the Kerguelen Plateau, whereas the lowest relative response was found at the HNLC station despite similar nutrient limitations. We hypothesize that acclimation of the local phytoplankton community to either frequent nutrient supply through winter mixing, causing a rapid doubling of the PP or, on the contrary, rare nutrient supply, induced an initial lag phase and thus a longer time laps before reaching a maximum response. Moreover, a wet rather than a dry deposition of aerosols in the HNLC area had minor effect on the net phytoplankton response, as only the less abundant pico- and nanoplankton groups responded more to a dry than a wet deposition, whereas the dominant diatom community responded equally to both deposition modes. However, we cannot exclude a bias caused by preferential grazing, as we did not remove zooplankton predators from the natural plankton community prior to the incubation experiments.

Further planned investigations on this dataset involve the study of dissolution and possible bioavailability of other trace elements such as Mn and Co dissolved from dust and ash particles (Fishwick et al., 2018) as these may limit phytoplankton growth in the open ocean (Mackey et al., 2012; Perron et al., 2020). Since the seasonal and spatial variability of organic matter concentration in surface seawater may impact nutrient dissolution and scavenging processes (de Leeuw et al., 2014), its influence on the response of phytoplankton to aerosol additions should

926 also be investigated (Bressac and Guieu, 2013; Hernández-Ruiz et al., 2020). Similarly, the
927 presence of ligands is known to play an important role on the bioavailability of trace elements
928 (Meskhidze et al., 2017; Paris and Desboeufs, 2013; Strzepek et al., 2011; Wagener et al., 2008).
929 Moreover, nutrient bioavailability in the SO may be disturbed in the future, according to climate
930 change predictions (Deppeler and Davidson, 2017). Hence, predicted changes in the SO for 2100
931 include an increase in surface temperature, as well as ocean acidification coupled to around twice
932 higher CO_2 concentrations. While dust deposition to the SO has doubled during the 20th century
933 (McConnell et al., 2007) and is thought to further increase, the pycnocline and MLD become
934 shallower (Deppeler and Davidson, 2017). Thus, more aerosols dissolve in a lower volume of
935 warmer, fresher and more acidic surface ocean, increasing PC (Deppeler and Davidson, 2017),
936 while the acidification is thought to impact nutrient solubility in general and Fe bioavailability in
937 particular (Trimborn et al., 2017 and references therein). Thus, further research is needed to
938 better constrain the evolution of aerosol burden and connected nutrient bioavailability in a
939 changing ocean.

940 **Acknowledgments**

941 The study has been financed by the French Research Program LEFE (Les Enveloppes Fluides et
942 l'Environnement) through BISOU and ITALIANO projects and by the DADDY project
943 supported by IPSL. We thank INSU and the French oceanographic fleet ('Flotte
944 océanographique française") for financial and logistic support to the OISO program and the
945 VT163/OISO-29 oceanographic campaign (https://doi.org/10.17600/18000972). We thank the
946 PACHIDERM analytical platform (LEMAR) for NOx and trace metal analysis; I. Djouraev
947 (LOCEAN) for ICP-MS analysis at the Alysés platform, IRD; M. Benrahmoune and F. Kaczmar
948 (LOCEAN) for managing clean labs and help in sample processing; F. Fu (LISA) for acid attack
949 of aerosols; M. Mandeng-Yogo (LOCEAN) for IR-MS and CN analysis at the Alysés platform,
950 IRD; S. Nowak (LISA) for XRS analysis at Paris Diderot University; I. Obernosterer and P.
951 Catala (LOMIC) for inter-comparison of flow cytometric data; L. Sicard (ITODYS) and M. Jean
952 Pierre (LISA) for nitrogen BET analysis and C. Vaulot (IS2M) for SSA for krypton BET
953 analysis.

Conflict of Interest

The authors declare no competing interests.

Data Availability Statement

The dataset is available in the supporting information Table S1 and at the address: https://www.seanoe.org/data/00696/80825/

References

Agusti, S., Lubián, L. M., Moreno-Ostos, E., Estrada, M. and Duarte, C. M.: Projected changes in photosynthetic picoplankton in a warmer subtropical ocean, Front. Mar. Sci., 5(JAN), 1–16, doi:10.3389/fmars.2018.00506, 2019.

Aminot, A. and Kérouel, R.: Dosage automatique des nutriments dans les eaux marines : méthodes en flux continu., 2007.

Ardyna, M., Lacour, L., Sergi, S., d'Ovidio, F., Sallée, J. B., Rembauville, M., Blain, S., Tagliabue, A., Schlitzer, R., Jeandel, C., Arrigo, K. R. and Claustre, H.: Hydrothermal vents trigger massive phytoplankton blooms in the Southern Ocean, Nat. Commun., 10(1), doi:10.1038/s41467-019-09973-6, 2019.

Armand, L. K., Cornet-Barthaux, V., Mosseri, J. and Quéguiner, B.: Late summer diatom biomass and community structure on and around the naturally iron-fertilised Kerguelen Plateau in the Southern Ocean, Deep Sea Res. Part II Top. Stud. Oceanogr., 55(5–7), 653–676, doi:10.1016/j.dsr2.2007.12.031, 2008.

Ayris, P. and Delmelle, P.: Volcanic and atmospheric controls on ash iron solubility: A review, Phys. Chem. Earth, 45–46, 103–112, doi:10.1016/j.pce.2011.04.013, 2012.

Baines, S., Twining, B. S., Brzezinski, M. A., Krause, J., Vogt, S., Assael, D. and McDaniel, H.: Significant silicon accumulation by marine picocyanobacteria, Nat. Geosci., 5(12), 886–891, doi:10.1038/ngeo1641, 2012.

Baker, A. R. and Jickells, T. D.: Mineral particle size as a control on aerosol iron solubility, Geophys. Res. Lett., 33(17), doi:10.1029/2006GL026557, 2006.

Blain, S., Sedwick, P. N., Griffiths, F. B., Quéguiner, B., Bucciarelli, E., Fiala, M., Pondaven, P. and Tréguer, P.: Quantification of algal iron requirements in the Subantarctic Southern Ocean (Indian sector), Deep. Res. Part II Top. Stud. Oceanogr., 49(16), 3255–3273, doi:10.1016/S0967-0645(02)00082-6, 2002.

Blain, S., Quéguiner, B., Armand, L. K., Belviso, S., Bombled, B., Bopp, L., Bowie, A. R., Brunet, C., Brussaard, C. P. D., Carlotti, F., Christaki, U., Corbière, A., Durand, I., Ebersbach, F., Fuda, J. L., Garcia, N., Gerringa, L., Griffiths, B., Guigue, C., Guillerm, C., Jacquet, S., Jeandel, C., Laan, P., Lefèvre, D., Lo Monaco, C., Malits, A., Mosseri, J., Obernosterer, I., Park,

989 Y. H., Picheral, M., Pondaven, P., Remenyi, T., Sandroni, V., Sarthou, G., Savoye, N.,
990 Scouarnec, L., Souhaut, M., Thuiller, D., Timmermans, K. R., Trull, T. W., Uitz, J., Van Beek,
991 P., Veldhuis, M., Vincent, D., Viollier, E., Vong, L. and Wagener, T.: Effect of natural iron
992 fertilization on carbon sequestration in the Southern Ocean, Nature, 446(7139), 1070–1074,
993 doi:10.1038/nature05700, 2007.
994 Blain, S., Sarthou, G. and Laan, P.: Distribution of dissolved iron during the natural iron-
995 fertilization experiment KEOPS (Kerguelen Plateau , Southern Ocean), , 55, 594–605,
996 doi:10.1016/j.dsr2.2007.12.028, 2008.
997 Bowie, A. R., Van Der Merwe, P., Quéroué, F., Trull, T., Fourquez, M., Planchon, F., Sarthou,
998 G., Chever, F., Townsend, A. T., Obernosterer, I., Sallée, J. B. and Blain, S.: Iron budgets for
999 three distinct biogeochemical sites around the Kerguelen Archipelago (Southern Ocean) during
1000 the natural fertilisation study, KEOPS-2, Biogeosciences, 12(14), 4421–4445, doi:10.5194/bg-
1001 12-4421-2015, 2015.
1002 Boyd, P. W., Jickells, T. D., Law, C. S., Blain, S., Boyle, E. A., Buesseler, K. O., Coale, K. H.,
1003 Cullen, J. J., De Baar, H. J. W., Follows, M., Harvey, M., Lancelot, C., Levasseur, M., Owens,
1004 N. P. J., Pollard, R., Rivkin, R. B., Sarmiento, J., Schoemann, V., Smetacek, V., Takeda, S.,
1005 Tsuda, A., Turner, S. and Watson, A. J.: Mesoscale iron enrichment experiments 1993-2005:
1006 Synthesis and future directions, Science (80-.)., 315(5812), 612–617,
1007 doi:10.1126/science.1131669, 2007.
1008 Boyd, P. W., Mackie, D. S. and Hunter, K. A.: Aerosol iron deposition to the surface ocean -
1009 Modes of iron supply and biological responses, Mar. Chem., 120(1–4), 128–143,
1010 doi:10.1016/j.marchem.2009.01.008, 2010.
1011 Bressac, M. and Guieu, C.: Post-depositional processes: What really happens to new atmospheric
1012 iron in the ocean's surface?, Global Biogeochem. Cycles, 27(3), 859–870,
1013 doi:10.1002/gbc.20076, 2013.
1014 Browning, T. J., Bouman, H. A., Henderson, G. M., Mather, T. A., Pyle, D. M., Schlosser, C.,
1015 Woodward, E. M. S. and Moore, C. M.: Strong responses of Southern Ocean phytoplankton
1016 communities to volcanic ash, Geophys. Res. Lett., 41(8), 2851–2857,
1017 doi:10.1002/2014GL059364, 2014.
1018 Browning, T. J., Achterberg, E. P., Rapp, I., Engel, A., Bertrand, E. M., Tagliabue, A. and
1019 Moore, C. M.: Nutrient co-limitation at the boundary of an oceanic gyre, Nature, 551(7679),
1020 242–246, doi:10.1038/nature24063, 2017.
1021 Brzezinski, M. A.: The Si:C:N ratio of marine diatoms: interspecific variability and the effect of
1022 some environmental variables, J. Phycol., 21(3), 347–357, doi:10.1111/j.0022-
1023 3646.1985.00347.x, 1985.
1024 Cassar, N., Bender, M. L., Barnett, B. A., Fan, S., Moxim, W. J., Levy, H. and Tilbrook, B.: The
1025 Soutern Ocean biological response to aeolian iron deposition, Science (80-.)., 317, 1067–1070,
1026 doi:10.1038/050458a0, 2007.
1027 Chester, R. and Jickells, T. D.: The transport of material to the oceans: the atmospheric pathway,
1028 in Marine Geochemistry, pp. 52–82., 2012.

Chever, F., Bucciarelli, E., Sarthou, G., Speich, S., Arhan, M., Penven, P. and Tagliabue, A.: Physical speciation of iron in the Atlantic sector of the Southern Ocean along a transect from the subtropical domain to the Weddell Sea Gyre, J. Geophys. Res. Ocean., 115(10), 1–15, doi:10.1029/2009JC005880, 2010.

Chou, L. and Wollast, R.: Steady-state kinetics and dissolution mechanisms of albite., Am. J. Sci., 285(10), 963–993, doi:10.2475/ajs.285.10.963, 1985.

Claquin, P., Martin-Jezequel, V., Kromkamp, J. C., Veldhuis, M. J. W. and Kraay, G. W.: Uncoupling of silicon compared with carbon and nitrogen metabolisms and the role of the cell cycle in continuous cultures of Thalassiosira pseudonana (Bacillariophyceae) under light, nitrogen, and phosphorus control, J. Phycol., 38(5), 922–930, doi:10.1046/j.1529-8817.2002.t01-1-01220.x, 2002.

Closset, I., Lasbleiz, M., Leblanc, K., Quéguiner, B., Cavagna, A. J., Elskens, M., Navez, J. and Cardinal, D.: Seasonal evolution of net and regenerated silica production around a natural Fe-fertilized area in the Southern Ocean estimated with Si isotopic approaches, Biogeosciences, 11(20), 5827–5846, doi:10.5194/bg-11-5827-2014, 2014.

Conway, T. M., Wolff, E. W., Rothlisberger, R., Mulvaney, R. and Elderfield, H. E.: Constraints on soluble aerosol iron flux to the Southern Ocean at the Last Glacial Maximum, Nat. Commun., 6, doi:10.1038/ncomms8850, 2015.

Cruz, B. N. and Neuer, S.: Heterotrophic Bacteria Enhance the Aggregation of the Marine Picocyanobacteria Prochlorococcus and Synechococcus, Front. Microbiol., 10, doi:10.3389/fmicb.2019.01864, 2019.

Deppeler, S. L. and Davidson, A. T.: Southern Ocean phytoplankton in a changing climate, Front. Mar. Sci., 4(FEB), doi:10.3389/fmars.2017.00040, 2017.

Desboeufs, K. V., Losno, R., Vimeux, F. and Cholbi, S.: The pH-dependent dissolution of wind-transported Saharan dust, J. Geophys. Res. Atmos., 104(D17), 21287–21299, doi:10.1029/1999JD900236, 1999.

Dugdale, R. C. and Wilkerson, F. P.: Silicate regulation of newproduction in the equatorial Pacific upwelling, Nature, 391, 270, doi:10.1038/246170a0, 1998.

Duggen, S., Croot, P. L., Schacht, U. and Hoffmann, L. J.: Subduction zone volcanic ash can fertilize the surface ocean and stimulate phytoplankton growth: Evidence from biogeochemical experiments and satellite data, Geophys. Res. Lett., doi:10.1029/2006GL027522, 2007.

Duggen, S., Olgun, N., Croot, P. L., Hoffmann, L. J., Dietze, H., Delmelle, P. and Teschner, C.: The role of airborne volcanic ash for the surface ocean biogeochemical iron-cycle: A review, Biogeosciences, 7(3), 827–844, doi:10.5194/bg-7-827-2010, 2010.

Durant, A. J., Bonadonna, C. and Horwell, C. J.: Atmospheric and environmental impacts of volcanic particulates, Elements, 6, 235–240, doi:10.2113/gselements.6.4.235, 2010.

Erickson, D. J., Hernandez, J. L., Ginoux, P., Gregg, W. W., McClain, C. and Christian, J.: Atmospheric iron delivery and surface ocean biological activity in the southern ocean and Patagonian region, Geophys. Res. Lett., 30(12), doi:10.1029/2003GL017241, 2003.

Estrada, M., Delgado, M., Blasco, D., Latasa, M., Cabello, A. M., Benítez-Barrios, V., Fraile-

Nuez, E., Mozetič, P. and Vidal, M.: Phytoplankton across tropical and subtropical regions of the Atlantic, Indian and Pacific oceans, PLoS One, 11(3), 1–29, doi:10.1371/journal.pone.0151699, 2016.

Fishwick, M. P., Ussher, S. J., Sedwick, P. N., Lohan, M. C., Worsfold, P. J., Buck, K. N. and Church, T. M.: Impact of surface ocean conditions and aerosol provenance on the dissolution of aerosol manganese, cobalt, nickel and lead in seawater, Mar. Chem., 198(October 2017), 28–43, doi:10.1016/j.marchem.2017.11.003, 2018.

Fripiat, F., Leblanc, K., Elskens, M., Cavagna, A. J., Armand, L. K., André, L., Dehairs, F. and Cardinal, D.: Efficient silicon recycling in summer in both the Polar Frontal and Subantarctic Zones of the Southern Ocean, Mar. Ecol. Prog. Ser., 435, 47–61, doi:10.3354/meps09237, 2011a.

Fripiat, F., Cavagna, A. J., Savoye, N., Dehairs, F., André, L. and Cardinal, D.: Isotopic constraints on the Si-biogeochemical cycle of the Antarctic Zone in the Kerguelen area (KEOPS), Mar. Chem., 123(1–4), 11–22, doi:10.1016/j.marchem.2010.08.005, 2011b.

Frogner, P., Reynir Gíslason, S. and Óskarsson, N.: Fertilizing potential of volcanic ash in ocean surface water, Geology, 29(6), 487, doi:10.1130/0091-7613(2001)029<0487:FPOVAI>2.0.CO;2, 2001.

Fu, F.: Etude des apports des métaux traces par le dépôt atmosphérique en Méditerranée occidentale, Université Paris Diderot - Paris VII., 2018.

Gassó, S. and Torres, O.: Temporal Characterization of Dust Activity in the Central Patagonia Desert (Years 1964–2017), J. Geophys. Res. Atmos., 124(6), 3417–3434, doi:10.1029/2018JD030209, 2019.

Gili, S., Gaiero, D. M., Goldstein, S. L., Chemale, F., Koester, E., Jweda, J., Vallelonga, P. and Kaplan, M. R.: Provenance of dust to Antarctica: A lead isotopic perspective, Geophys. Res. Lett., 43(5), 2291–2298, doi:10.1002/2016GL068244, 2016.

Grand, M. M., Measures, C. I., Hatta, M., Hiscock, W. T., Landing, W. M., Morton, P. L., Buck, C. S., Barrett, P. M. and Resing, J. A.: Dissolved Fe and Al in the upper 1000 m of the eastern Indian Ocean: A high-resolution transect along 95°E from the Antarctic margin to the Bay of Bengal, Global Biogeochem. Cycles, 29(3), 375–396, doi:10.1002/2014GB004920, 2015a.

Grand, M. M., Measures, C. I., Hatta, M., Morton, P. L., Barrett, P., Milne, A., Resing, J. A. and Landing, W. M.: The impact of circulation and dust deposition in controlling the distributions of dissolved Fe and Al in the south Indian subtropical gyre, Mar. Chem., 176, 110–125, doi:10.1016/j.marchem.2015.08.002, 2015b.

Grasshoff, K., Kremling, K. and Ehrhardt, M.: Methods of seawater analysis., 1999.

Gudmundsson, M. T., Thordarson, T., Hoskuldsson, A., Larsen, G., Bjornsson, H., Prata, F. J., Oddsson, B., Magnusson, E., Hognadottir, T., Petersen, G. N., Hayward, C. L., Stevenson, J. A. and Jonsdottir, I.: Ash generation and distribution from the April-May 2010 eruption of Eyjafjallajökull, Iceland, Sci. Rep., 2, 1–12, doi:10.1038/srep00572, 2012.

Guieu, C., Loÿe-Pilot, M. D., Ridame, C. and Thomas, C.: Chemical characterization of the Saharan dust end-member: Some biogeochemical implications for the western Mediterranean

1109 Sea, J. Geophys. Res. Atmos., 107(15), doi:10.1029/2001JD000582, 2002.
1110 Guieu, C., Dulac, F., Desboeufs, K. V., Wagener, T., Pulido-Villena, E., Grisoni, J. M., Louis,
1111 F., Ridame, C., Blain, S., Brunet, C., Bon Nguyen, E., Tran, S., Labiadh, M. and Dominici, J.
1112 M.: Large clean mesocosms and simulated dust deposition: A new methodology to investigate
1113 responses of marine oligotrophic ecosystems to atmospheric inputs, Biogeosciences, 7(9), 2765–
1114 2784, doi:10.5194/bg-7-2765-2010, 2010.
1115 Guieu, C., Dulac, F., Ridame, C. and Pondaven, P.: Introduction to project DUNE, a DUst
1116 experiment in a low Nutrient, low chlorophyll Ecosystem, Biogeosciences, 11(2), 425–442,
1117 doi:10.5194/bg-11-425-2014, 2014.
1118 Hassler, C. S., Schoemann, V., Nichols, C. M., Butler, E. C. V. and Boyd, P. W.: Saccharides
1119 enhance iron bioavailability to Southern Ocean phytoplankton, Proc. Natl. Acad. Sci., 108(3),
1120 1076–1081, doi:10.1073/pnas.1010963108, 2011.
1121 Hernández-Ruiz, M., Barber-Lluch, E., Prieto, A., Logares, R. and Teira, E.: Response of pico-
1122 nano-eukaryotes to inorganic and organic nutrient additions, Estuar. Coast. Shelf Sci., 235(May
1123 2019), doi:10.1016/j.ecss.2019.106565, 2020.
1124 Hoffmann, L. J., Peeken, I. and Lochte, K.: Iron, silicate, and light co-limitation of three
1125 Southern Ocean diatom species, Polar Biol., 31(9), 1067–1080, doi:10.1007/s00300-008-0448-6,
1126 2008.
1127 Hoffmann, L. J., Breitbarth, E., Ardelan, M. V., Duggen, S., Olgun, N., Hassellöv, M. and
1128 Wängberg, S. Å.: Influence of trace metal release from volcanic ash on growth of Thalassiosira
1129 pseudonana and Emiliania huxleyi, Mar. Chem., 132–133(March 2012), 28–33,
1130 doi:10.1016/j.marchem.2012.02.003, 2012.
1131 Hörstmann, C., Raes, E. J., Buttigieg, P. L., Lo Monaco, C., John, U. and Waite, A. M.:
1132 Hydrographic fronts shape productivity , nitrogen fixation , and microbial community
1133 composition in the South Indian Ocean and the Southern Ocean, Biogeociences Discuss.,
1134 (March), 1–32, doi:https://doi.org/10.5194/bg-2021-52, 2021.
1135 Hutchins, D. A., Sedwick, P. N., DiTullio, G. R., Boyd, P. W., Quéguiner, B., Griffiths, F. B.
1136 and Crossley, C.: Control of phytoplankton growth by iron and silicic acid availability in the
1137 subantarctic Southern Ocean: Experimental results from the SAZ Project, J. Geophys. Res.
1138 Ocean., 106(C12), 31559–31572, doi:10.1029/2000JC000333, 2001.
1139 Jabaud-Jan, A., Metzl, N., Brunet, C., Poisson, A. and Schauer, B.: Interannual variability of the
1140 carbon dioxide system in the southern Indian Ocean (20°S-60°S): The impact of a warm
1141 anomaly in austral summer 1998, Global Biogeochem. Cycles, 18(1),
1142 doi:10.1029/2002gb002017, 2004.
1143 Jacq, V.: Influence de la biodiversité des nutriments sur la fixation de N2 et réponse de
1144 Crocosphaera watsonii face à la limitation en fer, Université Pierre et Marie Curie - Paris VI.
1145 [online] Available from: https://tel.archives-ouvertes.fr/tel-01127359, 2014.
1146 Jickells, T. D., An, Z. S., Andersen, K. K., Baker, A. R., Bergametti, G., Brooks, N., Cao, J. J.,
1147 Boyd, P. W., Duce, R. A., Hunter, K. A., Kawahata, H., Kubilay, N., LaRoche, J., Liss, P. S.,
1148 Mahowald, N. M., Prospero, J. M., Ridgwell, A. J., Tegen, I. and Torres, R.: Global Iron

1149 Connections Between Desert Dust, Ocean Biogeochemistry, and Climate, Science (80-.)., 1150 308(5718), 67–71, doi:10.1126/science.1105959, 2005.
1151 Jones, M. T. and Gislason, S. R.: Rapid releases of metal salts and nutrients following the 1152 deposition of volcanic ash into aqueous environments, Geochim. Cosmochim. Acta, 72(15), 1153 3661–3680, doi:10.1016/j.gca.2008.05.030, 2008.
1154 Jordi, A., Basterretxea, G., Tovar-Sánchez, A., Alastuey, A. and Querol, X.: Copper aerosols 1155 inhibit phytoplankton growth in the Mediterranean Sea, Proc. Natl. Acad. Sci. U. S. A., 109(52), 1156 21246–21249, doi:10.1073/pnas.1207567110, 2012.
1157 Journet, E., Desboeufs, K. V., Caquineau, S. and Colin, J.-L.: Mineralogy as a critical factor of 1158 dust iron solubility, Geophys. Res. Lett., 35(7), n/a-n/a, doi:10.1029/2007GL031589, 2008.
1159 Krause, J. W., Brzezinski, M. A., Baines, S. B., Collier, J. L., Twining, B. S. and Ohnemus, D. 1160 C.: Picoplankton contribution to biogenic silica stocks and production rates in the Sargasso Sea, 1161 Global Biogeochem. Cycles, 31(5), 762–774, doi:10.1002/2017GB005619, 2017.
1162 Langmann, B.: Volcanic Ash versus Mineral Dust: Atmospheric Processing and Environmental 1163 and Climate Impacts, ISRN Atmos. Sci., 2013(ii), 1–17, doi:10.1155/2013/245076, 2013.
1164 Langmann, B., Zakšek, K. and Hort, M.: Atmospheric distribution and removal of volcanic ash 1165 after the eruption of Kasatochi volcano: A regional model study, J. Geophys. Res., 115(March), 1166 D00L06, doi:10.1029/2009JD013298, 2010a.
1167 Langmann, B., Zakšek, K., Hort, M. and Duggen, S.: Volcanic ash as fertiliser for the surface 1168 ocean, Atmos. Chem. Phys., 10(8), 3891–3899, doi:10.5194/acp-10-3891-2010, 2010b.
1169 de Leeuw, G., Guieu, C., Arneth, A., Bellouin, N., Bopp, L., Boyd, P. W., Denier van der Gon, 1170 H. A. C., Desboeufs, K. V., Dulac, F., Facchini, M. C., Gantt, B., Langmann, B., Mahowald, N. 1171 M., Marañón, E., O'Dowd, C., Olgun, N., Pulido-Villena, E., Rinaldi, M., Stephanou, E. G. and 1172 Wagener, T.: Ocean-atmosphere interactions of gases and particles, in Ocean-Atmosphere 1173 Interactions of Gases and Particles, pp. 1–315., 2014.
1174 Li, F., Ginoux, P. and Ramaswamy, V.: Distribution, transport, and deposition of mineral dust in 1175 the Southern Ocean and Antarctica: Contribution of major sources, J. Geophys. Res., 113(D10), 1176 D10207, doi:10.1029/2007JD009190, 2008.
1177 Liu, Y., Debeljak, P., Rembauville, M., Blain, S. and Obernosterer, I.: Diatoms shape the 1178 biogeography of heterotrophic prokaryotes in early spring in the Southern Ocean, Environ. 1179 Microbiol., 21(4), 1452–1465, doi:10.1111/1462-2920.14579, 2019.
1180 Mackey, K. R. M., Buck, K. N., Casey, J. R., Cid, A., Lomas, M. W., Sohrin, Y. and Paytan, A.: 1181 Phytoplankton responses to atmospheric metal deposition in the coastal and open-ocean Sargasso 1182 Sea, Front. Microbiol., 3(OCT), 1–15, doi:10.3389/fmicb.2012.00359, 2012.
1183 Mahowald, N. M.: Anthropocene changes in desert area: Sensitivity to climate model 1184 predictions, Geophys. Res. Lett., 34(18), 1–5, doi:10.1029/2007GL030472, 2007.
1185 Mahowald, N. M., Kohfeld, K., Hansson, M., Balkanski, Y., Harrison, S. P., Prentice, I. C., 1186 Schulz, M. and Rodhe, H.: Dust sources and deposition during the last glacial maximum and 1187 current climate: A comparison of model results with paleodata from ice cores and marine 1188 sediments, J. Geophys. Res. Atmos., 104(D13), 15895–15916, doi:10.1029/1999JD900084,

1999.
Marañón, E., Fernández, A., Mouriño-Carballido, B., MartÍnez-GarcÍa, S., Teira, E., Cermeño, P., Chouciño, P., Huete-Ortega, M., Fernández, E., Calvo-Díaz, A., Morán, X. A. G., Bode, A., Moreno-Ostos, E., Varela, M. M., Patey, M. D. and Achterberg, E. P.: Degree of oligotrophy controls the response of microbial plankton to Saharan dust, Limnol. Oceanogr., 55(6), 2339–2352, doi:10.4319/lo.2010.55.6.2339, 2010.
Marcotte, A. R., Anbar, A. D., Majestic, B. J. and Herckes, P.: Mineral Dust and Iron Solubility: Effects of Composition, Particle Size, and Surface Area, Atmosphere (Basel)., 11(5), 533, doi:10.3390/atmos11050533, 2020.
Marie, D., Partensky, F., Vaulot, D. and Brussaard, C.: Enumeration of Phytoplankton, Bacteria, and Viruses in Marine Samples, Curr. Protoc. Cytom., 10(1), doi:10.1002/0471142956.cy1111s10, 1999.
Martin, J. H.: Glacial-interglacial CO 2 change: The Iron Hypothesis, Paleoceanography, 5(1), 1–13, doi:10.1029/PA005i001p00001, 1990.
McClain, C. R., Signorini, S. R. and Christian, J. R.: Subtropical gyre variability observed by ocean-color satellites, Deep. Res. Part II Top. Stud. Oceanogr., 51(1–3), 281–301, doi:10.1016/j.dsr2.2003.08.002, 2004.
McConnell, J. R., Aristarain, A. J., Banta, J. R., Edwards, P. R. and Simões, J. C.: 20th-Century doubling in dust archived in an Antarctic Peninsula ice core parallels climate change and desertification in South America, Proc. Natl. Acad. Sci. U. S. A., 104(14), 5743–5748, doi:10.1073/pnas.0607657104, 2007.
Mélançon, J., Levasseur, M., Lizotte, M., Delmelle, P., Cullen, J., Hamme, R. C., Peña, A., Simpson, K. G., Scarratt, M., Tremblay, J. É., Zhou, J., Johnson, K., Sutherland, N., Arychuk, M., Nemcek, N. and Robert, M.: Early response of the northeast subarctic Pacific plankton assemblage to volcanic ash fertilization, Limnol. Oceanogr., 59(1), 55–67, doi:10.4319/lo.2014.59.1.0055, 2014.
Mélançon, J., Levasseur, M., Lizotte, M., Scarratt, M., Tremblay, J. É., Tortell, P., Yang, G. P., Shi, G. Y., Gao, H., Semeniuk, D., Robert, M., Arychuk, M., Johnson, K., Sutherland, N., Davelaar, M., Nemcek, N., Peña, A. and Richardson, W.: Impact of ocean acidification on phytoplankton assemblage, growth, and DMS production following Fe-dust additions in the NE Pacific high-nutrient, low-chlorophyll waters, Biogeosciences, 13(5), 1677–1692, doi:10.5194/bg-13-1677-2016, 2016.
Meskhidze, N., Nenes, A., Chameides, W. L., Luo, C. and Mahowald, N. M.: Atlantic Southern Ocean productivity: Fertilization from above or below?, Global Biogeochem. Cycles, 21(2), 1–9, doi:10.1029/2006GB002711, 2007.
Meskhidze, N., Hurley, D., Royalty, T. M. and Johnson, M. S.: Potential effect of atmospheric dissolved organic carbon on the iron solubility in seawater, Mar. Chem., 194(June), 124–132, doi:10.1016/j.marchem.2017.05.011, 2017.
Metzl, N. and Lo Monaco, C.: Surface underway measurements of partial pressure of carbon dioxide (pCO2), salinity, temperature and other associated parameters during the R/V Marion

Dufresne OISO-29 cruise (EXPOCODE 35MV20190109) in Indian Ocean from 2019-01-09 to 2019-02-08, NOAA Natl. Centers Environ. Information. Dataset [online] Available from: https://www.ncei.noaa.gov/access/metadata/landing-page/bin/iso?id=gov.noaa.nodc:0208441 (Accessed 24 March 2021), 2020.

Metzl, N., Brunet, C., Jabaud-Jan, A., Poisson, A. and Schauer, B.: Summer and winter air-sea CO2 fluxes in the Southern Ocean, Deep. Res. Part I Oceanogr. Res. Pap., 53(9), 1548–1563, doi:10.1016/j.dsr.2006.07.006, 2006.

Middag, R., De Baar, H. J. W., Laan, P., Cai, P. H. and van Ooijen, J. C.: Dissolved manganese in the Atlantic sector of the Southern Ocean, Deep. Res. Part II Top. Stud. Oceanogr., 58(25–26), 2661–2677, doi:10.1016/j.dsr2.2010.10.043, 2011.

Mills, M. M., Ridame, C., Davey, M., La Roche, J. and Geider, R. J.: Iron and phosphorus co-limit nitrogen fixation in the eastern tropical North Atlantic, Nature, 429(6989), 292–294, doi:10.1038/nature02550, 2004.

Moore, C. M., Seeyave, S., Hickman, A. E., Allen, J. T., Lucas, M. I., Planquette, H., Pollard, R. T. and Poulton, A. J.: Iron-light interactions during the CROZet natural iron bloom and EXport experiment (CROZEX) I: Phytoplankton growth and photophysiology, Deep. Res. Part II Top. Stud. Oceanogr., 54(18–20), 2045–2065, doi:10.1016/j.dsr2.2007.06.011, 2007.

Moore, J. K., Abbott, M. R. and Richman, J. G.: Location and dynamics of the Antarctic Polar Front from satellite sea surface temperature data, J. Geophys. Res. Ocean., 104(C2), 3059–3073, doi:10.1029/1998jc900032, 1999.

Moore, J. K., Doney, S. C., Glover, D. M. and Fung, I. Y.: Iron cycling and nutrient-limitation patterns in surface waters of the world ocean, Deep. Res. Part II Top. Stud. Oceanogr., 49(1–3), 463–507, doi:10.1016/S0967-0645(01)00109-6, 2002.

Morel, A., Claustre, H. and Gentili, B.: The most oligotrophic subtropical zones of the global ocean: Similarities and differences in terms of chlorophyll and yellow substance, Biogeosciences, 7(10), 3139–3151, doi:10.5194/bg-7-3139-2010, 2010.

Morin, G. P., Vigier, N. and Verney-Carron, A.: Enhanced dissolution of basaltic glass in brackish waters: Impact on biogeochemical cycles, Earth Planet. Sci. Lett., 417, 1–8, doi:10.1016/j.epsl.2015.02.005, 2015.

Mosseri, J., Quéguiner, B., Armand, L. K. and Cornet-Barthaux, V.: Impact of iron on silicon utilization by diatoms in the Southern Ocean: A case study of Si/N cycle decoupling in a naturally iron-enriched area, Deep. Res. Part II Top. Stud. Oceanogr., 55(5–7), 801–819, doi:10.1016/j.dsr2.2007.12.003, 2008.

Murphy, J. and Riley, J. P.: A modified single solution method for the determination of phosphate in natural waters, Anal. Chim. Acta, doi:10.1016/S0003-2670(00)88444-5, 1962.

Nelson, D. M., Brzezinski, M. A., Sigmon, D. and Franck, V.: A seasonal progression of Si limitation in the Pacific sector of the Southern Ocean, Deep Sea Res. Part II Top. Stud. Oceanogr., 48(19–20), 3973–3995, doi:10.1016/S0967-0645(01)00076-5, 2001.

Nunn, B. L., Faux, J. F., Hippmann, A. A., Maldonado, M. T., Harvey, H. R., Goodlett, D. R., Boyd, P. W. and Strzepek, R. F.: Diatom Proteomics Reveals Unique Acclimation Strategies to

Mitigate Fe Limitation, PLoS One, doi:10.1371/journal.pone.0075653, 2013.
Paris, R. and Desboeufs, K. V.: Effect of atmospheric organic complexation on iron-bearing dust solubility, Atmos. Chem. Phys., 13(9), 4895–4905, doi:10.5194/acp-13-4895-2013, 2013.
Paris, R., Desboeufs, K. V. and Journet, E.: Variability of dust iron solubility in atmospheric waters: Investigation of the role of oxalate organic complexation, Atmos. Environ., 45(36), 6510–6517, doi:10.1016/j.atmosenv.2011.08.068, 2011.
Paytan, A., Mackey, K. R. M., Chen, Y., Lima, I. D., Doney, S. C., Mahowald, N. M., Labiosa, R. and Post, A. F.: Toxicity of atmospheric aerosols on marine phytoplankton, Proc. Natl. Acad. Sci., 106(12), 4601–4605, doi:10.1073/pnas.0811486106, 2009.
Perron, M. M. G., Strzelec, M., Gault-Ringold, M., Proemse, B. C., Boyd, P. W. and Bowie, A. R.: Assessment of leaching protocols to determine the solubility of trace metals in aerosols, Talanta, 208, doi:10.1016/j.talanta.2019.120377, 2020.
Piketh, S. J., Tyson, P. D. and Steffen, W.: Aeolian transport from southern Africa and iron fertilization of marine biota in the South Indian Ocean, S. Afr. J. Sci., 96(May), 244–246 [online] Available from: https://hdl.handle.net/10520/AJA00382353_8986, 2000.
Planquette, H., Statham, P. J., Fones, G. R., Charette, M. A., Moore, C. M., Salter, I., Nédélec, F. H., Taylor, S. L., French, M., Baker, A. R., Mahowald, N. M. and Jickells, T. D.: Dissolved iron in the vicinity of the Crozet Islands, Southern Ocean, Deep. Res. Part II Top. Stud. Oceanogr., 54(18–20), 1999–2019, doi:10.1016/j.dsr2.2007.06.019, 2007.
Pye, H. O. T., Nenes, A., Alexander, B., Ault, A. P., Barth, M. C., Clegg, S. L., Collett Jr., J. L., Fahey, K. M., Hennigan, C. J., Herrmann, H., Kanakidou, M., Kelly, J. T., Ku, I.-T., McNeill, V. F., Riemer, N., Schaefer, T., Shi, G., Tilgner, A., Walker, J. T., Wang, T., Weber, R. J., Xing, J., Zaveri, R. A. and Zuend, A.: The acidity of atmospheric particles and clouds, Atmos. Chem. Phys., 20(8), 4809–4888, doi:10.5194/acp-20-4809-2020, 2020.
Ragueneau, O., Savoye, N., Del Amo, Y., Cotten, J., Tardiveau, B. and Leynaert, A.: A new method for the measurement of biogenic silica in suspended matter of coastal waters: Using Si:Al ratios to correct for the mineral interference, Cont. Shelf Res., 25(5–6), 697–710, doi:10.1016/j.csr.2004.09.017, 2005.
Ras, J., Claustre, H. and Uitz, J.: Spatial variability of phytoplankton pigment distributions in the Subtropical South Pacific Ocean: Comparison between in situ and predicted data, Biogeosciences, 5(2), 353–369, doi:10.5194/bg-5-353-2008, 2008.
Redfield, A. C.: On the proportions of organic derivatives in sea water and their relation to the composition of plankton, Univ. Press Liverpool, James John, 176–192, 1934.
Ridame, C., Dekaezemacker, J., Guieu, C., Bonnet, S., L'Helguen, S. and Malien, F.: Contrasted Saharan dust events in LNLC environments: Impact on nutrient dynamics and primary production, Biogeosciences, 11(17), 4783–4800, doi:10.5194/bg-11-4783-2014, 2014.
Rose, W. I. and Durant, A. J.: Fine ash content of explosive eruptions, J. Volcanol. Geotherm. Res., 186(1–2), 32–39, doi:10.1016/j.jvolgeores.2009.01.010, 2009.
Schlitzer, R.: Ocean Data View, [online] Available from: https://odv.awi.de, 2021.
Sedwick, P. N., Blain, S., Quéguiner, B., Griffiths, F. B., Fiala, M., Bucciarelli, E. and Denis,

M.: Resource limitation of phytoplankton growth in the Crozet Basin, Subantarctic Southern Ocean, Deep. Res. Part II Top. Stud. Oceanogr., 49(16), 3327–3349, doi:10.1016/S0967-0645(02)00086-3, 2002.

Shetye, S. S., Mohan, R. and Nair, A.: Latitudinal shifts in the Polar Front in Indian sector of the Southern Ocean: Evidences from silicoflagellate assemblage, Geosci. J., 18(2), 241–246, doi:10.1007/s12303-013-0061-8, 2014.

Shiro, N.: Nannoplankton flora in the Southern Ocean, with special reference to siliceous varieties, Mem. Natl. Inst. Polar Res. Spec. Issue, 40(40), 56–68, 1986.

Simonella, L. E., Palomeque, M. E., Croot, P. L., Stein, A., Kupczewski, M., Rosales, A., Montes, M. L., Colombo, F., García, M. G., Villarosa, G. and Gaiero, D. M.: Soluble iron inputs to the Southern Ocean through recent andesitic to rhyolitic volcanic ash eruptions from the Patagonian Andes, Global Biogeochem. Cycles, 29(8), 1125–1144, doi:10.1002/2015GB005177, 2015.

Smith, J., Vance, D., Kemp, R. A., Archer, C., Toms, P., King, M. and Zárate, M.: Isotopic constraints on the source of Argentinian loess – with implications for atmospheric circulation and the provenance of Antarctic dust during recent glacial maxima, Earth Planet. Sci. Lett., 212(1–2), 181–196, doi:10.1016/S0012-821X(03)00260-7, 2003.

Strzepek, R. F., Maldonado, M. T., Hunter, K. A., Frew, R. D. and Boyd, P. W.: Adaptive strategies by Southern Ocean phytoplankton to lessen iron limitation: Uptake of organically complexed iron and reduced cellular iron requirements, Limnol. Oceanogr., doi:10.4319/lo.2011.56.6.1983, 2011.

Tagliabue, A., Bopp, L. and Aumont, O.: Ocean biogeochemistry exhibits contrasting responses to a large scale reduction in dust deposition, Biogeosciences, 5(1), 11–24, doi:10.5194/bg-5-11-2008, 2008.

Tagliabue, A., Bowie, A. R., Boyd, P. W., Buck, K. N., Johnson, K. S. and Saito, M. A.: The integral role of iron in ocean biogeochemistry, Nature, 543(7643), 51–59, doi:10.1038/nature21058, 2017.

Taylor, S. R. and McLennan, S. M.: The continental crust: Its composition and evolution, edited by B. S. Publications, Blackwell Scientific Publications, Oxford. [online] Available from: https://www.osti.gov/biblio/6582885, 1985.

Tegen, I. and Schepanski, K.: Climate Feedback on Aerosol Emission and Atmospheric Concentrations, Curr. Clim. Chang. Reports, 4(1), doi:10.1007/s40641-018-0086-1, 2018.

Ternon, E., Guieu, C., Löye-Pilot, M. D., Leblond, N., Bosc, E., Gasser, B., Miquel, J. C. and Martín, J.: The impact of Saharan dust on the particulate export in the water column of the North Western Mediterranean Sea, Biogeosciences, 7(3), 809–826, doi:10.5194/bg-7-809-2010, 2010.

Thomalla, S. J., Waldron, H. N., Lucas, M. I., Read, J. F., Ansorge, I. J. and Pakhomov, E.: Phytoplankton distribution and nitrogen dynamics in the southwest indian subtropical gyre and Southern Ocean waters, Ocean Sci., 7(1), 113–127, doi:10.5194/os-7-113-2011, 2011.

Timmermans, K. R., Veldhuis, M. J. W., Laan, P. and Brussaard, C. P. D.: Probing natural iron fertilization near the Kerguelen (Southern Ocean) using natural phytoplankton assemblages and

1349 diatom cultures, Deep. Res. Part II Top. Stud. Oceanogr., 55(5–7), 693–705,
1350 doi:10.1016/j.dsr2.2007.12.008, 2008.
1351 Trimborn, S., Brenneis, T., Hoppe, C., Laglera, L., Norman, L., Santos-Echeandía, J., Völkner,
1352 C., Wolf-Gladrow, D. and Hassler, C. S.: Iron sources alter the response of Southern Ocean
1353 phytoplankton to ocean acidification, Mar. Ecol. Prog. Ser., 578, 35–50,
1354 doi:10.3354/meps12250, 2017.
1355 Twining, B. S., Rauschenberg, S., Baer, S. E., Lomas, M. W., Martiny, A. C. and Antipova, O.:
1356 A nutrient limitation mosaic in the eastern tropical Indian Ocean, Deep. Res. Part II Top. Stud.
1357 Oceanogr., 166(May), 125–140, doi:10.1016/j.dsr2.2019.05.001, 2019.
1358 Uitz, J., Claustre, H., Morel, A. and Hooker, S. B.: Vertical distribution of phytoplankton
1359 communities in open ocean: An assessment based on surface chlorophyll, J. Geophys. Res.,
1360 111(C8), C08005, doi:10.1029/2005JC003207, 2006.
1361 Uitz, J., Claustre, H., Griffiths, F. B., Ras, J., Garcia, N. and Sandroni, V.: A phytoplankton
1362 class-specific primary production model applied to the Kerguelen Islands region (Southern
1363 Ocean), Deep Sea Res. Part I Oceanogr. Res. Pap., 56(4), 541–560,
1364 doi:10.1016/j.dsr.2008.11.006, 2009.
1365 Vancoppenolle, M., Meiners, K. M., Michel, C., Bopp, L., Brabant, F., Carnat, G., Delille, B.,
1366 Lannuzel, D., Madec, G., Moreau, S., Tison, J.-L. and van der Merwe, P.: Role of sea ice in
1367 global biogeochemical cycles: emerging views and challenges, Quat. Sci. Rev., 79, 207–230,
1368 doi:10.1016/j.quascirev.2013.04.011, 2013.
1369 Wagener, T., Pulido-Villena, E. and Guieu, C.: Dust iron dissolution in seawater: Results from a
1370 one-year time-series in the Mediterranean Sea, Geophys. Res. Lett., 35(16), 1–6,
1371 doi:10.1029/2008GL034581, 2008.
1372 Watson, A. J., Bakker, D. C. E., Ridgwell, A. J., Boyd, P. W. and Law, C. S.: Effect of iron
1373 supply on Southern Ocean CO2 uptake and implications for glacial atmospheric CO2, Nature,
1374 407(6805), 730–733, doi:10.1038/35037561, 2000.
1375 Wei, Y., Sun, J., Chen, Z., Zhang, Z., Zhang, G. and Liu, X.: Significant contribution of
1376 picoplankton size fraction to biogenic silica standing stocks in the Western Pacific Ocean, Prog.
1377 Oceanogr., 192, 102516, doi:10.1016/j.pocean.2021.102516, 2021.
1378 Wiggert, J. D., Murtugudde, R. G. and Christian, J. R.: Annual ecosystem variability in the
1379 tropical Indian Ocean: Results of a coupled bio-physical ocean general circulation model, Deep
1380 Sea Res. Part II Top. Stud. Oceanogr., 53(5–7), 644–676, doi:10.1016/j.dsr2.2006.01.027, 2006.
1381 Witham, C. S., Oppenheimer, C. and Horwell, C. J.: Volcanic ash-leachates: a review and
1382 recommendations for sampling methods, J. Volcanol. Geotherm. Res., 141(3–4), 299–326,
1383 doi:10.1016/j.jvolgeores.2004.11.010, 2005.
1384 Wolff-Boenisch, D., Gislason, S. R. and Oelkers, E. H.: The effect of crystallinity on dissolution
1385 rates and CO2 consumption capacity of silicates, Geochim. Cosmochim. Acta, 70(4), 858–870,
1386 doi:10.1016/j.gca.2005.10.016, 2006.
1387 Wollast, R. and Chou, L.: Rate Control of Weathering of Silicate Minerals at Room Temperature
1388 and Pressure, in Physical and Chemical Weathering in Geochemical Cycles, pp. 11–32, Springer

1389 Netherlands, Dordrecht., 1988.
1390 Wuttig, K., Townsend, A. T., van der Merwe, P., Gault-Ringold, M., Holmes, T., Schallenberg,
1391 C., Latour, P., Tonnard, M., Rijkenberg, M. J. A., Lannuzel, D. and Bowie, A. R.: Critical
1392 evaluation of a seaFAST system for the analysis of trace metals in marine samples, Talanta,
1393 197(January), 653–668, doi:10.1016/j.talanta.2019.01.047, 2019.
1394